RELOCATING EARTHQUAKES BY HYPODD IN CINARCIK BASIN AND SURROUNDING

by

FATİH BULUT

B.S., Electronics, Marmara University

Submitted to

Boğaziçi University

Kandilli Observatory and Earthquake Research Institute

in partial fulfillment of

the requirements for the degree of

Master of Science

in

Geophysics

Boğaziçi University

2006

To my family...

ACKNOWLEDGMENTS

I would like to express my deepest thanks to my advisor, Prof. Dr. Mustafa Aktar. He provided me unlimited instruction and guidance in my studies. I thank him for his wisdom, patience, and continued support throughout my academic life.

The data set used in study is given by Hayrullah Karabulut. He also contributed this study by helpful discussions. I would like to thank him for his shares without any hesitation. I would like to thank KOERI, LGIT, IPGP and TUBITAK for providing seismic data.

Thanks go to the members of the Department of Geophysics at Boğaziçi University who have provided me the necessary atmosphere, instruction and support. Special thanks also go to Birsen Can. She has provided me incredible support in every stage of my studies. I would also like to thank Tuna Eken, Tülay Kaya, Özlem Kurtuluş and Dr.Gonca Örgülü for their frendships, supports and useful discussions.

My sincerest thanks go to my family. My father and mother, Mehmet and Kezban, have seen me through all situations in my life to help me reach this place. Thanks to my siblings, Nilgün, Nilay and Oğuzhan for supporting me and helping me have fun along the way. My wife, Necmiye, have provided me her support in every stage of my life. Her love is the most inevitable thing in my life. She will continue to be an inspiration to my presence.

ABSTRACT

We relocated part of aftershock activity in Çınarcık Basin and surrounding that are associated with the 1999 İzmit Earthquake M_w 7.4. We used double difference relocation algorithm (Waldhauser and Ellsworth, 2000) to relocate the aftershocks. The data set was obtained by a temporary seismic network deployed by Boğaziçi University, Kandilli Observatory and Earthquake Research Institute, LGIT (Grenoble) and IPGP (Paris) 10 days after the mainshock (Karabulut et al., 2002). For a better station coverage, additional data set was obtained from a network operated by TUBITAK Marmara Research Center. Differential travel times were calculated using both arrival time readings and waveform cross correlation method. We relocated 1550 of the aftershocks and interpreted the results by classification into three main clusters, namely, Tuzla, Yalova and Central Cluster. Tuzla Cluster is located in the northern scarp of the Çınarcık Basin and shows events that are linearly oriented in NW-SE direction. The depth section of this cluster indicates a vertically dipping activity,. The linear trend might imply a secondary strike-slip faulting parallel to the main one. However, the earlier fault plane solutions do not confirm this statement. Yalova Cluster contains a well-developed aftershock activity that is located beneath the north of the Armutlu Peninsula. The depth section of this activity reveals a well defined linearly dipping characteristic which is plunging to the north with an approximate angle of 56°. The orientation of the seismicity is roughly EW and therefore parallel to the main rupture of 1999 İzmit Earthquake. The Central Cluster traverses the total length of the Gulf of İzmit and extends into the Çınarcık Basin linearly with the orientation of E-W direction. It corresponds to the continuation of the main rupture of 1999 Izmit Earthquake to the west of the Hersek Peninsula. The relocation results obtained by HypoDD reveal seismicity patterns in a more clarified manner, provide more convincing data for models that were proposed before and finally imply new seismological ideas about the Eastern Marmara.

ÖZET

M_w 7.4 1999 İzmit Depremi ile ilişkili, Çınarcık Baseni ve çevresinde meydana gelen artçı deprem aktivitesini yeniden konumlandırdık. Artçı depremleri yeniden konumlandırmak için Double Difference Relocation (Waldhauser ve Ellsworth, 2000) algoritması kullanıldı. Veri seti, ana şoktan 10 gün sonra Boğaziçi Üniversitesi Kandilli Rasathanesi ve Deprem Araştırma Enstitüsü, LGIT (Grenoble) ve IPGP (Paris) tarafından kurulmuş geçici bir sismik ağ ile elde edilmiştir. Daha iyi bir istasyon çevrimi için ek bir veri seti, TUBITAK Marmara Araştırma Merkezi tarafından işletilen bir ağ tarafından elde edilmiştir. Diferansiyel yolculuk süreleri, hem varış zamanı okumalarından, hemde dalga formu çapraz ilişki metodu kullanılarak hesaplanmıştır. Artçı depremlerin 1550 tanesini yeniden konumlandırdık ve sonuçları, Tuzla, Yalova ve Merkez Küme şeklinde isimlendirerek sınıflandırdık. Tuzla Kümesi Çınarcık Baseni'nin kuzey uçurumunda yer almaktadır ve kuzeybatı-güneygoğu doğrultusunda doğrusal olarak yönelmiş olayları içermektedir. Bu kümenin derinlik kesiti dik olarak dalan bir aktivite göstererek muhtemelen esas faya paralel ikincil bir doğrultu atımlı faylanmayı ima eder. Yalova Kümesi Armutlu Yarımadası'nın kuzeyinde yera alan, çok iyi gelişmiş bir artçı deprem aktivitesi içerir. Bu aktivitenin derinlik kesiti, yaklaşık 56^{o} lik bir açıyla iyi bir şekilde tanımlanmış kuzeye doğru dalan bir yapı gösterir. Bu sistemin yönlenimi kabaca doğu-batı yönünde ve bu nedenle 1999 İzmit Depremi'nin esas kırığına paralellik gösterir. Merkez Küme, İzmit Körfezi'ni doğrusal olarak ortadan kesen ve doğu-batı doğrultusunda yönelenerek Çınarcık Baseni'ne doğru uzanan bir deprem aktivitesidir. Hersek Yarımadası'nın batısında 1999 İzmit Depremi'nin esas kırığının devamına karşılık gelir. HypoDD ile elde edilen yeniden konumlandırma sonuçları, sismik desenleri çok daha açık, anlaşılır bir manada gösterir ve Doğu Marmara ile ilgili yeni sismotektonik delililler ortaya koyar.

TABLE OF CONTENTS

ACKNOWLEDGEMENTS iv
ABSTRACT v
ÖZET vi
TABLE OF CONTENTS vii
LIST OF FIGURES ix
LIST OF TABLES xii

1. INTRODUCTION 1
2. SEISMICITY OF CINARCIK BASIN 4
   2.1. Tectonic Settings 4
   2.2. Previous Studies 6
3. ADVANCED EARTHQUAKE LOCATION PROCEDURES 11
   3.1. Review Of Earthquake Location 11
   3.2. Advanced Techniques 13
   3.3. Relocation Based On Doublets 14
4. INVESTIGATION of DOUBLE DIFFERENCE METHOD 16
   4.1. Basic Principle 16
      4.1.1. Statement of the Inverse Problem 16
      4.1.2. Solution of the Inverse Problem 19
      4.1.3. Experimenting with simple models 24
   4.2 Delay Measurement 27
      4.2.1. Time Domain Approach: Cross-correlation 28
         4.2.1.1 Basic Definitions 28
         4.2.1.2. Experiments 29
      4.2.2. Frequency Domain Approach: Cross-Spectral density 33
         4.2.1.1 Basic Definitions 33
         4.2.1.2. Experiments 35
   4.3 Testing HypoDD with Synthetic Data 38
5. RELOCATION OBTAINED BY DOUBLE DIFFERENCE METHOD 44

5.1. Tuzla Cluster 48
5.2. Yalova Cluster 51
5.3. Central Cluster 54
6. DISCUSSION and CONCLUSION 57
REFERENCES 64

LIST OF FIGURES

Page No

Figure 2.1 The complete bathymetric map of the Marmara Sea (Le Pichon et al., 2001) 5

Figure 2.2 Focal mechanism solutions using RMT method (Örgülü and Aktar, 2001)........ 7

Figure 2.3 Focal mechanism solutions (Karabulut et al., 2002) 8

Figure 2.4 (a) Aftershock distribution of the events having uncertainty less than 5 km, (b) Focal mechanism solutions of selected events (Özalaybey et al., 2002) 9

Figure 2.5 Hypocenters of the aftershocks until the end of September 1999 (Ito et al., 2002) 10

Figure 4.1 Open and solid circles represent the earthquakes. Red stars show the final position of relocated events indicated by open circles. Solid and dashed lines represent well and poor links, respectively. For event *i* and *j* the corresponding slowness vectors with respect to the station *k* are S_{ik} and S_{jk}, respectively. Arrows $\Delta \mathbf{m}_i$ and $\Delta \mathbf{m}_j$ indicate the relocation vector for event *i* and *j*. 17

Figure 4.2. Illustration of ray path in three dimensional spaces 19

Figure 4.3 Singular values of G matrix for the first case 25

Figure 4.4 Singular values of G matrix for the second case... 26

Figure 4.5 Singular values of G matrix for the last case 27

Figure 4.6 The Figures at the top are; the signals (a), the calculated correlation function (b) and the peak value of cross correlation (c).......... 31

Figure 4.7 The signals used in the investigation of interpolation and cross correlation approach.......... 32

Figure 4.8 The general view (a) and the view of the peak value (b) of correlogram.......... 32

Figure 4.9 The general view (a) and the view of the peak value (b) of correlogram.......... 33

Figure 4.10. The signals used in the experiment.......... 36

Figure 4.11. Amplitude spectrum (a) and phase spectrum (b) of cross spectral density..... 37

Figure 4.12 The velocity models used in synthetic test.......... 38

Figure 4.13 (a) Depth sections of the original events, (b) the events located by HYPOCENTER and (c) the events relocated by HypoDD. Note the improvement brought by HypoDD.......... 41

Figure 4.14 Epicenters of the original events (a), the events located by HYPOCENTER (b) and the events relocated by HYPODD (c).......... 42

Figure 5.1 The seismicity in the Eastern Marmara, starting 10 days after the 17 August 1999 Izmit Earthquake and lasting for 20 days (red circles) (locations taken from Karabulut et al, 2002). Grey triangles represent the stations used in this study. Tuzla, Central and Yalova clusters are indicated by red, blue and green rectangles, respectively.......... 45

Figure 5.2 For Tuzla cluster, the epicentral locations and depth view of (a) the initial model given by Karabulut et al, 2002 and (b) relocation results.......... 48

Figure 5.3 The epicentral location and detailed depth section of (a and c) the initial model given by Karabulut et al, 2002 and (b and d) relocation results 50

Figure 5.4 For Yalova cluster, the epicentral locations and depth views of (a) the initial model given by Karabulut et al, 2002, (b) relocation results (c) and relocation results on topographic map 52

Figure 5.5 The epicentral location and detailed depth section of (a and c) the initial model given by Karabulut et al, 2002 and (b and d) relocation results 54

Figure 5.6 For Central cluster, the epicentral locations and depth views of (a) the initial model given by Karabulut et al, 2002 and (b) relocation results 55

Figure 5.7 For Central cluster, the epicentral locations and detailed depth section of (a and c) the initial model given by Karabulut et al, 2002 and (b and d) relocation results 56

Figure 6.1 HypoDD relocation results of Tuzla and Central Clusters on bathymetric map. Fault lines are taken from Le Pichon et al., 2001 60

Figure 6.2 HypoDD relocation results of Yalova Cluster on topographic map: white circles and black lines represent the thermal springs and normal faults, respectively (Eisenlohr, 1997) 60

LIST OF TABLES

Page No

Table 5.1 One Dimensional Velocity Model 46

1. INTRODUCTION

One of the most damaging earthquakes of the last century occurred on 17 August 1999, which brings about a great concern in the society, in Turkey. The rupture of the main shock, 7.4 in M_W, extends to the west into the Marmara Sea and to the 20 km east of Düzce, on the North Anatolian Fault Zone (NAFZ). The continuation of the aftershock activity into the Marmara Sea plays an important role on the recognition of fault geometries and the tectonics of the region.

Many studies have been carried out with the aim of inspecting the seismicity associated with the 17 August 1999 Izmit earthquake. (i.e., Örgülü and Aktar, 2001 ; Karabulut et al., 2002; Özalaybey et al., 2002; Ito et al., 2002). The resolution of the studies shows that the aftershock distribution should be revised to present more accurate implications about the tectonic structures in the region, especially in the Marmara Sea.

The methods, based on one-dimensional velocity models, locate the events without the effects of three-dimensional velocity structure. These routine location methods also utilize the arrival readings obtained by picking the P and S phases on the seismograms. Therefore, arrival time reading accuracy, knowledge of the crustal structure and the network geometry are very important factors affecting the accuracy of hypocenter location.

In this study, we have inspected and used the double difference earthquake location method that is developed by Waldhauser and Ellsworth, (2000) to reduce the source of error caused by both arrival time reading and unmodeled velocity structure. The location method incorporates arrival readings depending on travel-time measurements and/or differential travel-time measurements obtained by cross-correlation of P- and S-wave.

The rays approximately travel the same path if the earthquakes occur very near to each other relative to the event-station distance. Travel time difference is also approximately independent on the unmodeled velocity structure along the ray paths from the events to the station. In such cases, travel time difference of two events recorded at one station can be regarded as the offset between this event pair in three-dimensional space. The double difference algorithm relocates the events by attempting to minimize these time differences for event pairs.

Even though the arrival times provide the travel time difference of the events, in order to improve the accuracy of delay measurement, waveform cross-correlation method should be applied to the P and S phase windows. Recent studies show that very precise hypocenter determinations with high resolution can be derived from waveform cross correlation data (i.e., San Andreas Fault by Rubin et al. [1999], Hayward fault by Waldhauser and Ellsworth [2002], Calaveras fault by Schaff et al. [2002], and Long Valley Caldera by Prejean et al. [2002]). Besides the cross-correlation in time domain (Deichmann and Garcia Fernandez, 1992), cross-spectral density is another method to measure the time differences, which is applied in frequency domain (Poupinet et al., 1984).

We relocated the events based on the data set prepared using both catalog and waveform based time difference measurements. We have investigated the delay measurement methods. There are two types of delay measurement approach, namely, cross correlation and cross spectral density. In this study, we adopted cross correlation approach in order to prepare the waveform based data set.

We have examined the basic principles of the method in detail using experiments based on synthetically generated data sets. In these experiments, the event geometry was kept simple but systematically modified according to the problems that needed to be analyzed. For any particular source geometry, the behavior of the inverse problems was investigated numerically.

The observational data set was obtained from a temporary local network, installed around the Eastern Marmara Sea 10 days after the beginning of the seismic sequence (Karabulut et al, 2002). For a better coverage, they combined additional data from the stations operated by the TUBITAK Marmara Research Center (Özalaybey et al, 2002). The observation period starts 10 days after the 17 August 1999 İzmit earthquake and lasts 15 days. We relocated 1550 of the aftershocks in the region surrounding the Çınarcık Basin using the double-difference

(HypoDD) earthquake relocation algorithm (Waldhauser and Ellsworth, 2000). The data set included both travel time readings and cross-correlation of P and S phase windows.

2. THE SEICMICITY OF ÇINARCIK BASIN

2.1 Tectonics

The North Anatolian fault zone (NAF) forms part of the boundary between Eurasian and African-Arabian plates starting from the Karliova Junction in the east and lasting to the Aegan Sea in the west. It is roughly 1500 km long, seismically active, right lateral transform fault that is located along the northern margin of the Anatolian Plate. The NAF cannot be traced further west than the North of the Aegan Sea. Barka explained this by decrease in the slip rate towards the west along the fault zone (1992). The seismicity of NAF creates one ore more major earthquakes per decades which migrated from the east to the west during the last century (Parsons et al., 2000). Eight large earthquakes occurred on the 800 km of its morphological trace, which are progressively migrating to the west (Armijo et al., 2002). GPS measurements (Reilenger et al., 2000) and seismic activities show that the Anatolian plate is moving to the west as a large block (about 18-25 mm/yr, Reilenger et al., 2000).

There is an active debate about when this fault zone first became active. Some authors argue that it was created in the late Miocene to Pliocene (Ketin, 1976; Şengör, 1979; Barka 1992). Ketin has claimed that it has horizontally displaced about 800-1000 m since the Quetarnary (1969) and a few tens of km since the Pliocene (1969). However, debates are still continuing about the actual cumulative displacement which occurred along the NAF.

In the Marmara region, the NAF is divided into three main strands. The southern strand goes through Yenişehir and Edremit. The central strand goes through the southern coastline of the Marmara Sea, Geyve and Bandırma, and enters to Aegan Sea passing Bayramic. The northern strand of the NAF enters the Sea of Marmara along the axis of the Gulf of Izmit. All the strands of the NAF in the Marmara Region change their strike directions form east-west to northeast-southwest at about 27.5^{o}E (Wong et al, 1995).

Inside the Marmara Sea, there are different explanations concerning the geometry of the NAF. According to Okay et al. (2000), it mainly consists of three different fault segments that are called North Boundary (45 km long), Central Marmara (105 km) and Ganos (15 km) faults, respectively. However, Le Pichon treats the Central Marmara and the North Boundary Faults as a single fault, called Main Marmara fault, which follows the deep basins which are aligned along axis of the Marmara Sea (2001).

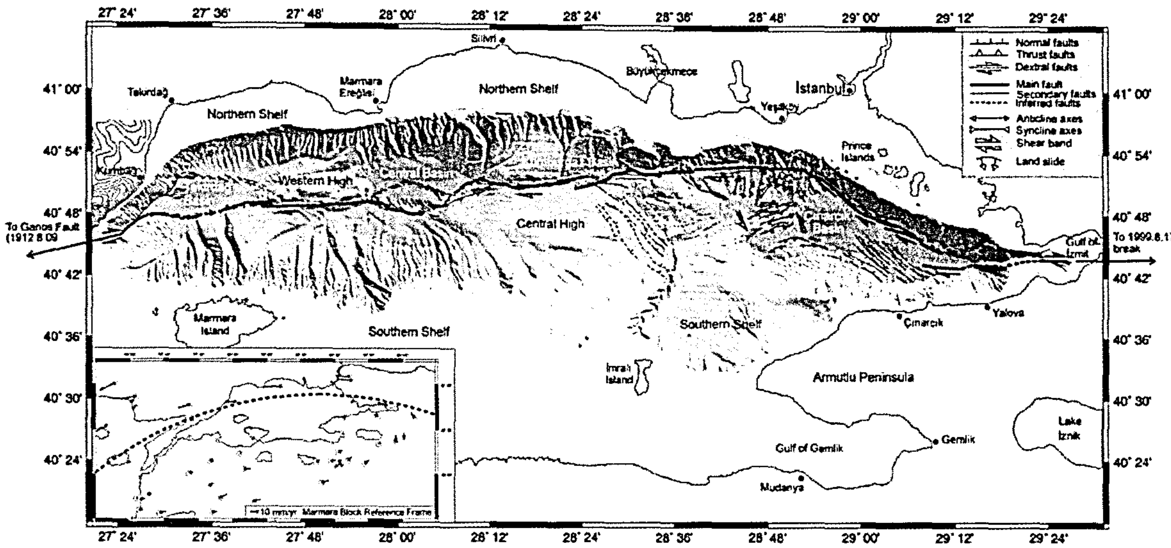

Figure 2.1 The complete bathymetric map of the Marmara Sea (Le Pichon et al., 2001)

According to Armijo et al. (2002), the north Marmara fault system involves oblique extension and it is segmented. His arguments are mostly based on the existence of rhomb shaped depressions which are characteristics of pull-apart basins. This complex geometry is also supported by relatively smaller size historical earthquakes. Therefore, Armijo et al. (2002) argue that the northern Marmara fault system includes significant fault step-overs that could terminate propagation of large seismic ruptures. This opinion is contradictory with the single purely strike-slip model of Le Pichon et al (2001). Le Pichon et al. (2001) claims that a single fault system nearly bisects the Marmara Trough. It connects the Izmit segment, which is ruptured during the M_W 7.4 İzmit Earthquake on 17.8.1999, to the Ganos fault, which is ruptured during the 1912 Şarköy-Mürefte earthquake.

There are three deep marine basins that constitute part of the Marmara Sea. From the east to the west, they are called Çınarcık Basin (maximum depth 1276 km), Central Basin (1265 km) and Tekirdağ Basin (1152 km), respectively. Those basins are separated by sill areas that rise about 600 above their surroundings (Wong et al, 1995). In this study, we focused on the seismicity of the Çınarcık Basin.

The Çınarcık basin is the most complicated part of the Main Marmara Fault. The eastern part of the basin is characterized by transtension and the western margin of the basin by strong transpression (Le Pichon et al., 2001). It is the widest as well as the deepest basin in the Marmara Sea, which is about 50 km-long, up to 20 km wide. It is filled with Pliocene and Quaternary sediments thicker than 3 km (Okay et al., 2000).

The North Boundary Fault is the section that joins the Central Marmara Fault in the west to the İzmit segment in the east, which is ruptured during the M_W 7.4 İzmit Earthquake on 17.8.1999 (Okay et al., 2000). The fault plane solutions of the strong aftershocks of the 1999 Izmit Earthquake beneath the northern boundary of the Çınarcık Basin (Örgülü and Aktar, 2001) imply existence of right lateral fault structures. There are northwest striking and very gently northeast-concave faults on the region that is called Çınarcık extensional field by Le Pichon et al., 2001. The southern margin of the Çınarcık basin is relatively irregular and less steep. The southern boundary is therefore more diffuse and covers a wide zone of about 10 km. The fault plane solutions dominantly indicate normal faulting located in the southern boundary of the Çınarcık Basin (Örgülü and Aktar, 2001, Özalaybey et al., 2002). The western margin of the basin dominantly consists of a series of thrust faults and folds against the Central high. Their strikes and trends are nearly aligned in north-south orientation (Le Pichon et al., 2001).

2.2 Previous Studies

Örgülü and Aktar analyzed the focal mechanisms of the strong aftershocks of 1999 İzmit earthquake ($4.0<M_L<6.2$) in Marmara Region. They provided thirty fault plane solutions by applying Regional Moment Tensor inversion method (RMT). They also support the fault plane solutions with the first polarity based solutions. Results of the study shows that the main characteristics of the 1999 Izmit Earthquake dominates the strong aftershocks as strike slip faulting. In the Marmara Sea, the fault plane solutions clearly show an existence a right lateral strike slip fault structure beneath the northern boundary of the Çınarcık Basin that is taken into consideration for the continuation of the NAF. The fault plane solutions of the events located in the north of the Armutlu Peninsula strongly indicate the existence of normal faulting. Örgülü and Aktar (2001) consider this activity to be a distinct segment along the northern coastline of the Armutlu Peninsula.

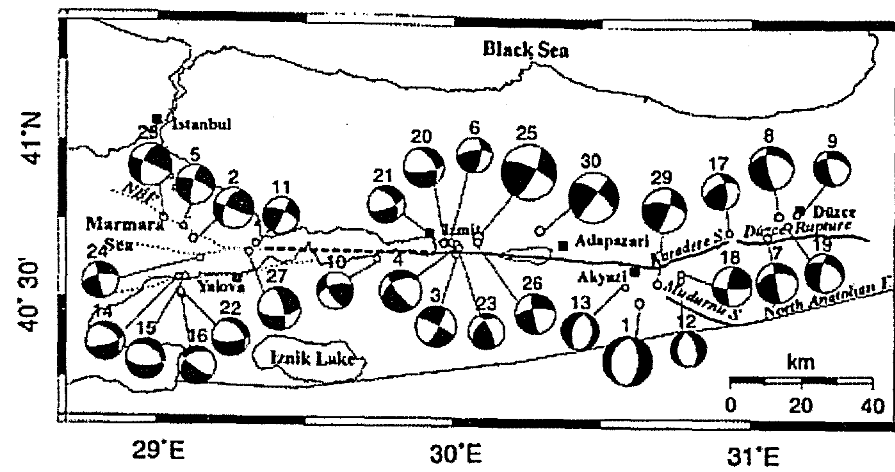

Figure 2.2 Focal mechanism solutions using RMT method (Örgülü and Aktar, 2001)

Karabulut et al. (2002) have investigated the aftershock activity of 1999 Izmit earthquake in Eastern Marmara Sea in terms of three main cluster, called Central, Yalova and Tuzla Clusters. They provided the location of the events which have been selected considering horizontal and vertical uncertainties less than 2.0 and 3.0 km, respectively. Karabulut et al. (2002) have also resolved the fault mechanisms of the events, which have magnitudes greater than 1.7, based on first motion polarities. The majority of the mechanisms in Central cluster correspond to E–W trending, right-lateral strike-slip faulting. This result is consistent with the seismicity and the mechanism of the mainshock. The activity of the cluster beneath the Armutlu peninsula is well-developed. It dips to the north with the angle of roughly 50°. Normal faulting mechanisms dominate this cluster mostly striking in the E–W direction and dipping 40°–65° N that confirms the dipping geometry of aftershock distribution. Karabulut et al. (2002) indicates the presence of hydrothermal fields in Armutlu peninsula that might be the reason of the shallow events. The activity located on a few km southwest of Tuzla does not show a clear lineament with a circular geometry in the map view. The majority of the fault plane solutions are NW–SE- and NNW–SSE-trending normal faulting. This cluster is considered by Karabulut et al. (2002) to be originated from a secondary faulting developed parallel to the Çınarcık Basin. It was shown that the focal mechanism solutions indicate two different stress regimes. These are normal faulting at shallow depths and strike-slip faulting at greater depths.

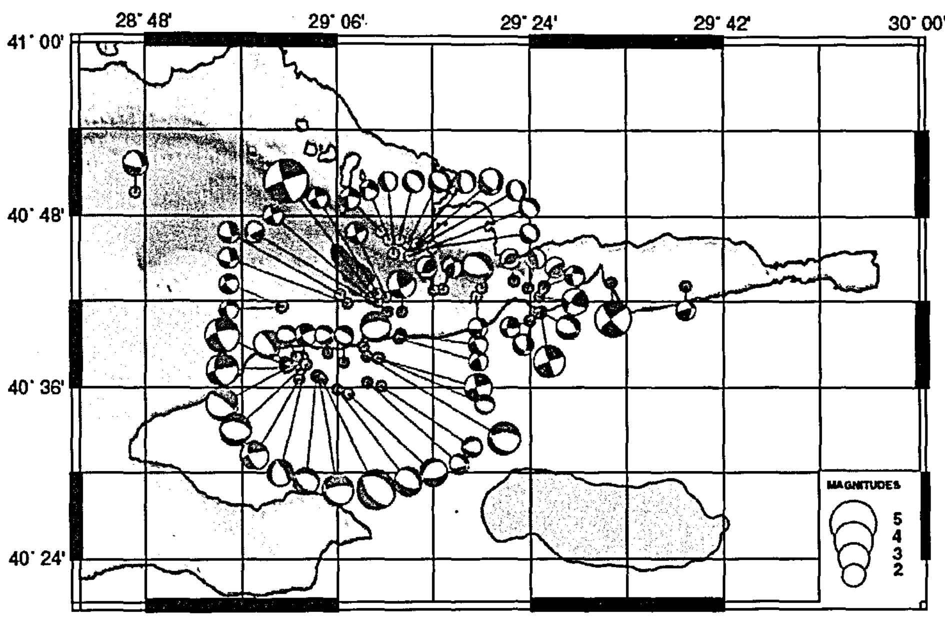

Figure 2.4 Focal mechanism solutions (Karabulut et al., 2002)

Özalaybey et al. (2002) provided the aftershock distribution of the 1999 İzmit Earthquake by using data obtained from a network consisting of 54 stations operated by the Earth Sciences Research Institute (ESRI) of the Marmara Research Center, TUBITAK. They have also listed the fault plane solutions of the large aftershocks (M_L>3.5), which were resolved based on the first motion polarities. Aftershock activity provided is almost entirely located offshore, extending along the Gulf of İzmit. The activity shows that the rupture reached 10 km south of the Princes Islands in the west. It was shown by Özalaybey et al. (2002) that the activity in Yalova Cluster is triggered by the complex redistribution of stresses and dynamic strains imposed by the dislocation of the mainshock. The fault plane solutions show that the dominant characteristic of the main branch of the rupture is right lateral strike slip. Beneath the northern scarp of the Çınarcık basin, the focal mechanisms keep the dominant characteristic of the rupture, whereas the focal mechanisms of the events that are located on the Yalova cluster are resolved to be normal fault.

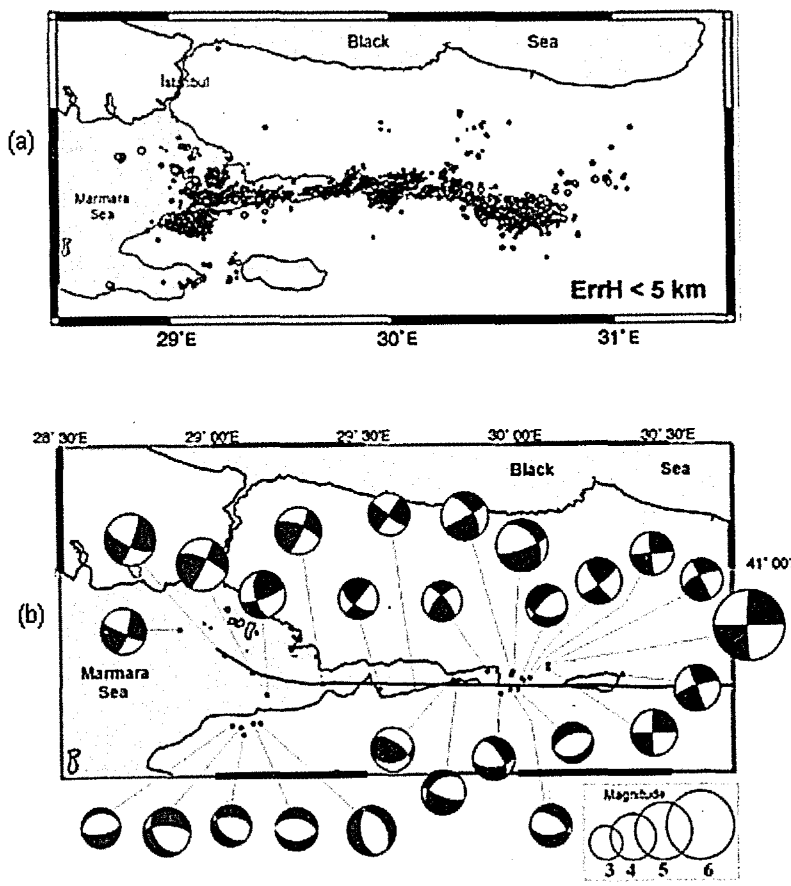

Figure 2.3 (a) Aftershock distribution of the events having uncertainty less than 5 km. (b) Focal mechanism solutions and fault rupture line are from Özalaybey et al. (2002)

Ito et al. (2002) provided the aftershock distribution of the 1999 Izmit earthquake that was obtained by using data from a local seismic network, IZINET, and 10 temporary seismic stations. More than 2000 aftershocks were located for the period of about 2 months following the mainshock. The uncertainty of the hypocenter is about 2 km horizontally and 3 km vertically. They provided several outcomes about the characteristics of the mainshock considering this aftershock distribution. Firstly, the rupture of the main shock initiated fault from a location adjacent to an active swarm area where many micro earthquakes had been occurring for more than 20 year prior to the main shock. Secondly, the aftershock region is extended in the east-west direction along the NAF, confirming the geometry of the main shock. Thirdly, the western end of the rupture caused by the main shock is likely to have reached up to about 29.2° E in the İzmit Bay, and hence the total length of the rupture caused by the mainshock is about 150 km, as long as the estimate of the fault rupture length is based on the aftershock distribution.

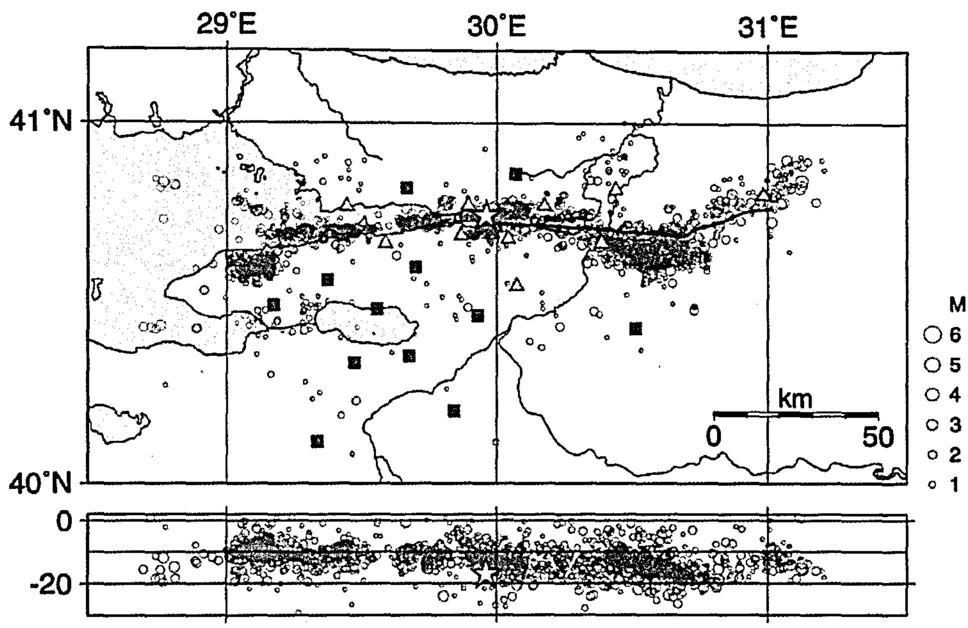

Figure 2.2 Hypocenters of the aftershocks until the end of September 1999 (Ito et al., 2002)

3. ADVANCED EARTHQUAKE LOCATION PROCEDURES

3.1. Review of Earthquake Location

Locating the earthquakes requires arrival time readings of available seismic phases, as well as velocity structure of the region between the events and the stations. If we know the location of an earthquake, we can calculate the travel time of an event at a station using any velocity model. This is the forward view of the inverse problem that we encounter while locating the earthquakes.

We aim to define the unknown parameters of an earthquake location, which are Cartesian coordinates and origin time of the earthquake, using the arrival times and the velocity model. In order to investigate the nature of the inverse problem, we assume that the velocity model is homogenous. With this assumption, the arrival time at the ith station, t_i, can be formulated as:

$$t_i = t_{origin} + \frac{\sqrt{(x_i - x)^2 + (y_i - y)^2 + (z_i - z)^2}}{v} \tag{3.1}$$

The Cartesian coordinates of the hypocenter and those of the ith station are x, y, z and x_i, y_i, z_i, respectively. It is obvious that there is a nonlinear relationship between coordinates and arrival time that needs to be linearized in order to solve the equation using classical inversion approaches. Let all the unknown parameters of location, x_i, y_i, z_i and t_{origin} be defined in a vector **m**. The problem is expressed in a simpler notation:

$$\mathbf{F(m) = d} \tag{3.2}$$

where **F** is a general non-linear operator that links the vector of unknown variables (**m**) to the data vector (**d**). All of the changes in **m** during the solution are approximated by Taylor series approximation with δm increments as given in equation (3.3). Let us assume that m_0 is the first step in the approximation and m_1 is the next one:

$$m_1 = m_0 + \delta m \tag{3.3}$$

The changes tend to solve the equation if they provide a better fit to the data space. During the solution process, the small modifications to the model vector are represented by δm which consist of $\delta t_0 = t_1 - t_0$, $\delta x_0 = x_1 - x_0$, $\delta y_0 = y_1 - y_0$ and $\delta z_0 = z_1 - z_0$. The corresponding change in the predicted data vector can be found by imposing (3.3) in a Taylor series expansion. Neglecting all terms which include higher order of the differential terms (i.e. linear approximation) of the model vector;

$$\left(\frac{\partial F}{\partial x_0}\right)\delta x_0 + \left(\frac{\partial F}{\partial y_0}\right)\delta y_0 + \left(\frac{\partial F}{\partial z_0}\right)\delta z_0 + \left(\frac{\partial F}{\partial t_0}\right)\delta t_0 = d - F_0(x_0, y_0, z_0, t_0) \qquad (3.4)$$

The combination of all linear equations (3.4) for all observations defines an inverse problem. The partial derivatives of **F** on the left hand side of (3.4) build the **G** matrix as given in the equation (3.5) below. Defining a new data vector as:

$$\mathbf{d} = d - F_0$$

the equation 3.4 can be written as::

$$\mathbf{Gm} = \mathbf{d} \qquad (3.5)$$

In this notation (3.5), **m** expresses the unknown model parameters that are expected to converge to the true values and d is the data vector, which is attempted to fit during the inversion. Due to the Taylor approximation, the solution takes a number of iteration to find the model parameters that are expected to cover the true ones. The inversion process continues until the data is fit acceptably. Unfortunately, the rate at which it converges to the true model parameters depends strongly on the accuracy of initial guess called the starting model (Lay and Wallace, 1995).

Past experience has shown that the inversion procedure described above is quite efficient in most situations and it has been used extensively throughout the world in a wide variety of seismological observations. Recently, as the number of observations and their quality have improved significantly, modern approaches were developed in order to increase the accuracy as well as the sensitivity of the earthquake locations process. A short review of the recently developed approaches is given in the next section.

3.2 Advanced Techniques

The new improvements in earthquake location techniques are based on three different concepts: new solution methods to the inverse problem, use of the three dimensional velocity models and relative location in multiple event clusters. In this section, we will mention some of the modern approaches involved in seismic event location.

Improvement in the solution of inverse problem: As an example of this class of solutions we will mention a constrained nonlinear simplex optimization technique (Rabinowitz, 1988) that falls into the class of grid search methods. We know that the poor arrival data sets lead the inverse problem to be ill conditioned, therefore numerically unstable. This method is more efficient than the standard derivative based algorithms if the arrivals can be detected at only a few receivers. The standard location algorithms usually truncate the inversion the small eigenvalues and many iterations update the adjustment solution vector using less than the full parameter space dimension, which may often leads to incorrect solutions. The location algorithm mentioned above utilizes flexible tolerance method that takes into account the nonlinear constrains and may improves the convergence in analyzing poorly constrained events.

Use of the three dimensional velocity models: The accuracy of techniques for travel time calculation is an essential part of the methods of seismic event location. A wide variety of methods has been developed in the last few decades. The one of most important developments in travel time calculation rises from the studies that aim to define the three dimensional velocity models. There are many methods for calculation of travel times considering three dimensional earth models that vary from each other with their computation strategies. The methods determine the solutions using the ray equations, however they may differ in using the Huygen's principle, Fermat's principle or the Eikonal equation. In basic principle, the interested region is separated to cells for which the velocity is supposed to be identified. The ray paths that are assumed to go through all of the cells are calculated. The behavior of the rays in each cell can be characterized by shooting or bending approaches.

The solution to the inverse problem based on 3-D velocity structures can be designed using either derivative based linear methods (Thurber, 1983) or nonlinear global search methods (Lomax, 1995). The main difficulty of the methods attempting to use the three dimensional structures is that they all require high quality travel time data.

3.3 Location Techniques based on Doublets

The third class of modern methods that is used in earthquake location is the relative location in multiple event clusters. This approach constitutes the main topic treated in this thesis and therefore is described in more detail. In the following we briefly introduce four main approaches that are based on relative location.

True doublets would be earthquakes that occurred at the same location at different dates and having the same magnitude (Poupinet et al., 1984). The earthquakes can be considered to be doublet if the hypocentral separation between them is very small in comparison with the event-station distance. This assumption allows us to measure the differential travel time of events using cross correlation owing to the similarity in waveforms.

Various type of earthquake relocation methods persist based on differential travel time measurements. The first one is the master event approach assuming that the location of an event in a cluster is known exactly and called master event, and the other events of the cluster can be relocated relative to the master event. (Ito, 1985; Van Decar and Crosson, 1990; Deichmann and Garcia-Fernandez, 1992; Lees, 1998; Pujol, 1992). The necessity of selecting master event leads to limitation for measurement of differential travel time using waveform cross correlation. If the other events of the cluster are not located sufficiently near to the master event, similarity in waveforms is reduced dramatically. That is why the clusters require to be separated to sub-clusters having different master events. The variety of master events at sub-clusters causes propagation of location errors from different sub-master events into the main cluster.

The limitation of master event approach was overcome by Got et al (1994), calculating cross-correlation delays for all possible event pairs and imposing them into one system of linear equations in order to be solved by least-squares methods to determine hypocentral separations. In this approach, the slowness vector to each station is considered similar to each other for all events of the cluster. Because only the waveform cross correlation data is used, uncorrelated events cannot be relocated by this method.

Another relocation method is suggested by Dodge et al (1995) called joint hypocenter determination method (JHD). In this approach, time difference measurements derived from master event approach are converted to phase picks, and hypocentral parameters, velocity model and station corrections are inverted simultaneously. This approach allows groups of correlated events with accurate interevent distances to move relative to one another by weaker constraints. In order to retain the accuracy of the cross correlation data, it is assumed that the events are clustered in a small volume so that the unmodeled velocity structure can be completely absorbed in the station corrections (Waldhauser, 2000).

Double difference is an efficient earthquake relocation technique that provides the simultaneous relocation of large numbers of earthquakes. It utilizes P- and S-wave differential travel times obtained from cross correlation methods with travel-time differences obtained from catalog data. Double difference algorithm minimizes residual differences for event pairs by adjusting the vector difference between their hypocenters. It allows us to determine interevent distances between correlated events that form a single multiplet to the accuracy of the cross-correlation data while simultaneously determining the relative locations of other multiplets and uncorrelated events to the accuracy of the catalog travel-time data, without the use of station corrections (Waldhauser, 2000).

4. INVESTIGATION of DOUBLE DIFFERENCE METHOD

4.1. Basic Principles

4.1.1. Statement of Inverse Problem

In this section, we will introduce the derivation of the earthquake relocation technique called double difference algorithm, developed by Waldhauser and Ellsworth (2000). The first step is to formulate the arrival time measurement of an event at a receiver.

$$T_k^i = \tau^i + \int_i^k u ds \tag{4.1}$$

Using ray theory, the arrival time, T, is expressed as a path integral along the ray path starting from the i^{th} earthquake to the k^{th} receiver. The origin time of event i is expressed by τ^i, u is the slowness field, and ds is the element of the path length. As mentioned in section 3.1, the relationship between the travel time and Cartesian coordinates of earthquake location is nonlinear. The relationship is linearized using Taylor series expansion (Geiger, 1910):

$$\frac{\partial t_k^i}{\partial m} \Delta m^i = r_k^i \tag{4.2}$$

where $r_k^i = (t^{obs} - t^{cal})_k^i$ is the difference between observed and calculated travel time and $\Delta m^i = (\Delta x^i, \Delta y^i, \Delta z^i, \Delta \tau^i)$ is the difference in hypocentral parameters of the event that fit the residual represented by r_k^i. The arrival time readings as given in equation (4.2), can be used to locate the earthquakes independently in the conventional way. However, the use of relative arrival time measurements for earthquake location requires taking the difference between two equations of the form (4.2) corresponding to an event pair (Fréchet, 1985),

$$\frac{\partial t_k^{ij}}{\partial m} \Delta m^{ij} = dr_k^{ij} \tag{4.3}$$

where $\Delta m^{ij} = (\Delta x^{ij}, \Delta y^{ij}, \Delta z^{ij}, \Delta \tau^{ij})$ is the difference in hypocentral parameters of the event pair and $dr_k^{ij} = (t^{obs} - t^{cal})_k^i - (t^{obs} - t^{cal})_k^j$ is the travel time difference of events i and j recorded at station k. The partial derivatives of the travel time t of each event with respect to m are calculated using the components of the slowness vector of the ray connecting the source to the receiver.

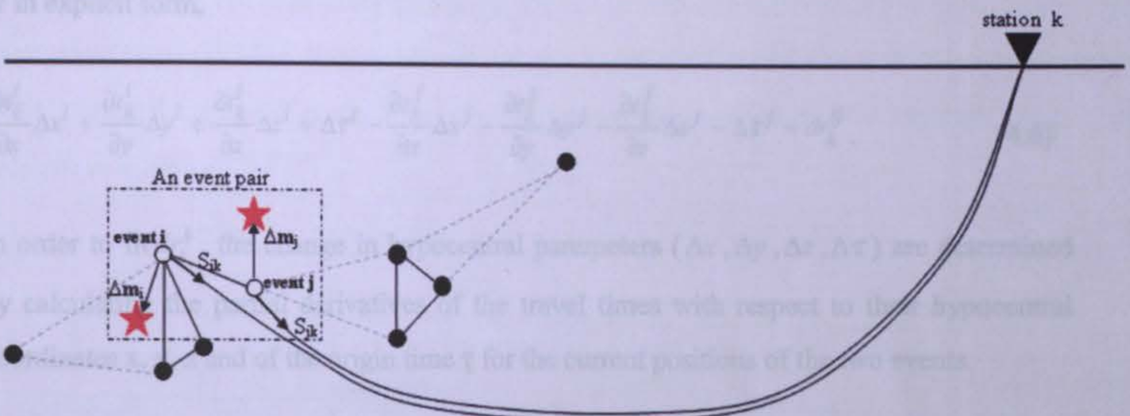

Figure 4.1. Open and solid circles represent the earthquakes. Red stars show the final position of relocated events indicated by open circles. Solid and dashed lines represent well and poor links, respectively. For event i and j the corresponding slowness vectors with respect to the station k are S_{ik} and S_{jk}, respectively. Arrows $\Delta\mathbf{m}_i$ and $\Delta\mathbf{m}_j$ indicate the relocation vector for event i and j.

Double difference algorithm works properly if the events are sufficiently close to each other allowing us to assume that the slowness vectors of each event are similar as indicated in Figure 4.1.

In equation (4.4), dr_k^{ij} is also represented as the residual between observed and theoretical differential time of two events.

$$dr_k^{ij} = (t_k^i - t_k^j)^{obs} - (t_k^i - t_k^j)^{cal} \tag{4.4}$$

The equation (4.4) is called the double difference equation. It should be obvious that time difference between i^{th} and j^{th} events observed at k^{th} receiver, $(t_k^i - t_k^j)^{obs}$, can be calculated either using arrival time readings or waveform cross correlations.

The equation (4.3) might be also written as:

$$\frac{\partial t_k^i}{\partial m}\Delta m^i - \frac{\partial t_k^j}{\partial m}\Delta m^j = dr_k^{ij} \qquad (4.5)$$

or in explicit form,

$$\frac{\partial t_k^i}{\partial x}\Delta x^i + \frac{\partial t_k^i}{\partial y}\Delta y^i + \frac{\partial t_k^i}{\partial z}\Delta z^i + \Delta\tau^i - \frac{\partial t_k^j}{\partial x}\Delta x^j - \frac{\partial t_k^j}{\partial y}\Delta y^j - \frac{\partial t_k^j}{\partial z}\Delta z^j - \Delta\tau^j = dr_k^{ij}. \qquad (4.6)$$

In order to fit dr_k^{ij}, the change in hypocentral parameters ($\Delta x, \Delta y, \Delta z, \Delta\tau$) are determined by calculating the partial derivatives of the travel times with respect to their hypocentral coordinates x, y, z and of the origin time τ for the current positions of the two events.

The combination of many linear equations of the form (4.6), given by a multitude of event pairs, forms an inverse problem as, as illustrated in Figure 4.1:

$$\mathbf{Gm} = \mathbf{d} \qquad (4.7)$$

where **G** is M x 4N matrix (M is the number of double difference observations, N is the number of events) containing partial derivatives, and **d** is the data vector containing the double difference observations.

In addition, the mean correction of all earthquakes is constrained to zero increasing number of rows of the equation (4.7) by four new equalities. These are expressed as:

$$\sum_{i=1}^{N} \Delta\mathbf{m}_i = 0 \qquad (4.8)$$

for each three coordinate direction and the origin time, making a total of four different additional equations

4.1.2. Solution of the Inverse Problem

Calculating the partial derivatives requires the information of take off and azimuth angles of the ray connecting the events and the stations. The epicentral coordinates of the events and the stations allow us to easily determine the azimuth angle (θ). However, the calculation of the take-off angle (ϕ) requires a numerical approach. Double difference algorithm adopts the method of false position that calculates the horizontal distance of travel in the event layer in order to find the take-off angle. Figure 4.2 illustrates the position and the ray path of an event relative to a station.

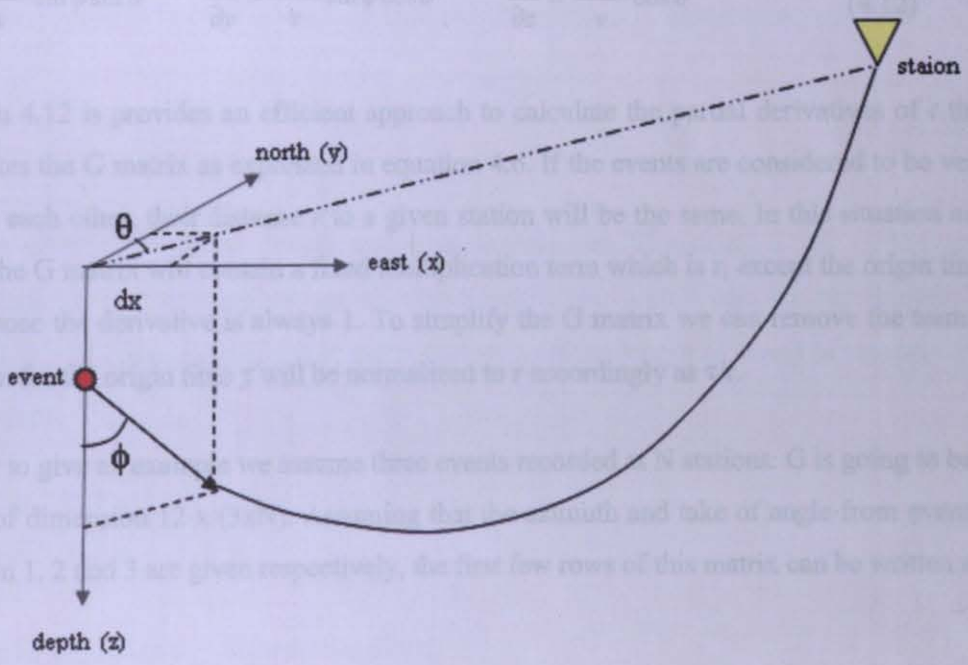

Figure 4.2

Let us consider a very small increment of the ray path that is emerging from the source. The duration elapsed at this increment can be expressed as;

$$t = \frac{r}{v} \tag{4.9}$$

where v is the velocity that is considered to be constant around the event. The length of increment, r, is;

$$r=\sqrt{x^2+y^2+z^2} \tag{4.10}$$

the partial derivatives of t are;

$$\frac{\partial t}{\partial x}=\frac{2x}{v\sqrt{r}} \qquad \frac{\partial t}{\partial y}=\frac{2y}{v\sqrt{r}} \qquad \frac{\partial t}{\partial z}=\frac{2z}{v\sqrt{r}} \tag{4.11}$$

The projections of the increment onto the spatial axes allow us to analytically define the partial derivatives in terms of ϕ and θ as:

$$\frac{\partial t}{\partial x}=\frac{2\sqrt{r}}{v}\sin\phi\sin\theta \qquad \frac{\partial t}{\partial y}=\frac{2\sqrt{r}}{v}\sin\phi\cos\theta \qquad \frac{\partial t}{\partial z}=\frac{2\sqrt{r}}{v}\cos\theta \tag{4.12}$$

Equation 4.12 is provides an efficient approach to calculate the partial derivatives of t that constitutes the **G** matrix as expressed in equation 4.6. If the events are considered to be very close to each other, their distance r to a given station will be the same. In this situation any row of the G matrix will contain a fixed multiplication term which is r, except the origin time term whose the derivative is always 1. To simplify the G matrix we can remove the term r. The term for the origin time τ will be normalized to r accordingly as τ/r.

In order to give an example we assume three events recorded at N stations. G is going to be a matrix of dimension 12 x (3xN). Assuming that the azimuth and take of angle from event 1 to station 1, 2 and 3 are given respectively, the first few rows of this matrix can be written as;

$$\begin{bmatrix}
\sin\phi_1^1\sin\theta_1^1 & \sin\phi_1^1\cos\theta_1^1 & \cos\phi_1^1 & 1 & -\sin\phi_1^2\sin\theta_1^2 & -\sin\phi_1^2\cos\theta_1^2 & -\cos\phi_1^2 & -1 & 0 & 0 & 0 & 0 \\
\sin\phi_1^1\sin\theta_1^1 & \sin\phi_1^1\cos\theta_1^1 & \cos\phi_1^1 & 1 & 0 & 0 & 0 & 0 & -\sin\phi_1^3\sin\theta_1^3 & -\sin\phi_1^3\cos\theta_1^3 & -\cos\phi_1^3 & -1 \\
0 & 0 & 0 & 0 & \sin\phi_1^2\sin\theta_1^2 & \sin\phi_1^2\cos\theta_1^2 & \cos\phi_1^2 & 1 & -\sin\phi_1^3\sin\theta_1^3 & -\sin\phi_1^3\cos\theta_1^3 & -\cos\phi_1^3 & -1 \\
\sin\phi_2^1\sin\theta_2^1 & \sin\phi_2^1\cos\theta_2^1 & \cos\phi_2^1 & 1 & -\sin\phi_2^2\sin\theta_2^2 & -\sin\phi_2^2\cos\theta_2^2 & -\cos\phi_2^2 & -1 & 0 & 0 & 0 & 0 \\
\sin\phi_2^1\sin\theta_2^1 & \sin\phi_2^1\cos\theta_2^1 & \cos\phi_2^1 & 1 & 0 & 0 & 0 & 0 & -\sin\phi_2^3\sin\theta_2^3 & -\sin\phi_2^3\cos\theta_2^3 & -\cos\phi_2^3 & -1
\end{bmatrix}$$

Subscripts and superscripts represent station and event ids, respectively.

Due to the nature of the problem, **G** is a sparse matrix containing only 8 nonzero elements for each row, representing the partial derivatives of the hypocentral parameters of an event pair with respect to a single station (equation 4.6).

The connection between two events is more valid if they have sufficiently small interevent distances in comparison to the distance between the events and the station. In such cases, the system of linear equation is well conditioned and is possible to be solved by the Singular Value Decomposition (SVD). Because of the sparseness of **G** matrix, the size of the system should be small to be solved by SVD approach.

Since **G** matrix is not a square matrix and has a size of N x M, it cannot be decomposed into eigenvectors and eigenvalues. First, we will construct a square matrix (4.13) containing **G** and $\mathbf{G}^T$ in order to define the problem in terms of eigenvalues. A new matrix is defined:

$$\mathbf{S} = \begin{bmatrix} \mathbf{0} & \mathbf{G} \\ \mathbf{G}^{\mathrm{T}} & \mathbf{0} \end{bmatrix} \tag{4.13}$$

The size of **S** is (N+M) x (N+M), and it is symmetrical. Therefore, S has (N+M) real eigenvalues λ_i and a complete set of eigenvectors, $\mathbf{w}_i$, which can be represented as $\mathbf{S}\mathbf{w}_i = \lambda_i \mathbf{w}_i$. By separating $\mathbf{w}_i$ into $\mathbf{u}_i$ and $\mathbf{v}_i$ vectors, with the length of N and M respectively, we can write:

$$\mathbf{S}\mathbf{w} = \begin{bmatrix} \mathbf{0} & \mathbf{G} \\ \mathbf{G}^{\mathrm{T}} & \mathbf{0} \end{bmatrix} \begin{bmatrix} \mathbf{u}_i \\ \mathbf{v}_i \end{bmatrix} = \lambda_i \begin{bmatrix} \mathbf{u}_i \\ \mathbf{v}_i \end{bmatrix} \tag{4.14}$$

This can be written as two separate identities:

$$\mathbf{G}\mathbf{v}_i = \lambda_i \mathbf{u}_i \quad \text{i=1,..,M} \tag{4.15}$$

and

$$\mathbf{G}^{\mathrm{T}}\mathbf{u}_i = \lambda_i \mathbf{v}_i \quad \text{i=1,..,N} \tag{4.16}$$

In matrix form, equation (4.15) can be written as,

$$\mathbf{GV} = \Lambda \mathbf{U} \tag{4.17}$$

Λ is a diagonal matrix containing M+N eigenvalues, called the singular values. Because of **S** being a Hermitian matrix, **U** and **V** are orthogonal to $\mathbf{U}^T$ and $\mathbf{V}^T$, respectively.

$$\mathbf{S} = \mathbf{S}^H, \mathbf{UU}^T = \mathbf{I}, \mathbf{VV}^T = \mathbf{I} \tag{4.18}$$

By multiplying equation (4.17) by $\mathbf{V}^T$, the singular value decomposition is derived as;

$$\mathbf{G} = \mathbf{U}\Lambda\mathbf{V}^T \tag{4.19}$$

The equation (4.19), allows any rectangular matrix to be described in terms of eigenvalues and eigenvectors. The elements of diagonal singular value matrix usually decrease continuously converging to zero, moreover, some of the values of the diagonal might be zero as well. In such cases, Λ is partitioned into a sub matrix, Λ_p, containing p singular values and several zero matrices as,

$$\Lambda = \begin{bmatrix} \Lambda_p & 0 \\ 0 & 0 \end{bmatrix} \tag{4.20}$$

Λ_p is a $p \times p$ diagonal matrix containing nonzero singular values. The equation (4.19) then becomes;

$$\mathbf{G} = \mathbf{U}\Lambda\mathbf{V}^T = \mathbf{U}_p\Lambda_p\mathbf{V}_p{}^T \tag{4.21}$$

That is why the other portion of **U** and **V** are canceled by the zeros of Λ. The equation $\mathbf{Gm} = \mathbf{d}$ is also represented as

$$\mathbf{U}_p\Lambda_p\mathbf{V}_p{}^T\mathbf{m} = \mathbf{d} \tag{4.22}$$

Therefore, the natural solution to the inverse problem, $\mathbf{m}^{est}$, can be constructed from singular value decomposition as;

$$\mathbf{m}^{est} = \mathbf{V}_p \Lambda_p^{-1} \mathbf{U}_p{}^T \mathbf{d} \tag{4.23}$$

The events, which are poorly related to others, lead **G** to be ill conditioned, thus, the stability of the system dramatically falls down due to the reduction in the number of non-zero singular values. One method to deal with this problem is to take the poorly linked events out of the equation system. The solution is performed by only well linked event pairs that are observed more than the minimum observation number. As known, the observation number is dependent on the network geometry and event distribution.

Another method to regularize the ill conditioned **G** matrix is the damped least squares solution. The equation system is first weighted by diagonal weighting matrix, **W**, based on the quality of double difference observations. Weighting is often useful in order to take into account the fact that some observations are made with more accuracy than others. The weighting matrix is constructed using either arrival time reading quality for catalog data or correlation coefficient for waveform cross correlation data. A classical solution to the equation (4.7) with a weighted least squares approach is

$$\mathbf{m}^{est} = \left[\mathbf{G}^T \mathbf{W} \mathbf{G}\right]^{-1} \mathbf{G}^T \mathbf{W} \mathbf{d} \tag{4.24}$$

d is the data vector , and **W** is weighting matrix based on the quality of the data.

The second step in the solution is to get rid of the singular values which are zero. Instead of defining G matrix by non-zero singular values only, it is possible to use all of them by damping the smaller ones with a small number, **e**. Then the equation (4.24) becomes;

$$\mathbf{m}^{est} = \left[\mathbf{G}^T \mathbf{W} \mathbf{G} + \mathbf{e}^2 \mathbf{I}\right]^{-1} \mathbf{G}^T \mathbf{W} \mathbf{d} \tag{4.25}$$

This change has a little effect on the large singular values but prevents the smaller singular values from leading to large variance (Menke, 1989). Whereas variance of the system was improved by damping, still its solution is not natural because its data and model resolution are reduced. Since there is not a simple method to determine what **e** should be, it must be determined by trial and error.

4.1.3. Experimenting with Simple Models

In this part, in order to inspect the behavior of the inverse problem posed by double difference method, we construct a **G** matrix as introduced in the section 4.1.2. We use a relatively simple model where a given number of events closely located are observed by a given number of stations at roughly the same distance around the cluster. We form the matrix in an analytical way considering the simple geometry of the problem. All of the variables in the G matrix, including the partial derivatives are given by simple trigonometric relations. The partial derivatives were calculated using take off and azimuth angles of rays connecting the events and the stations. The ray path of events can be regarded as slightly different if the interevent distance is very small relative to the distance between events and stations. With this approach, the azimuth and take off angles of events, which are recorded at the same station, can be defined with small variations.

We also inverted G matrix using SVD that is introduced in the section 4.1.2. As known, the inverse problem would be underdetermined if the number of equations were smaller than the unknown model parameters. In double difference problem, there are eight unknown model parameters for each linear equation. Therefore, we need eight or more equations for each event pair in order to handle the nonuniqueness of the model parameters. However, it is not possible to get full rank without imposing a priori information expressed by equation (4.8) because of the nature of double difference problem.

In the experiment, we aimed to exhibit the effect of azimuthal distribution of the stations on the solution of inverse problem of the double difference method. We set different models consisting of three events that are covered by four, six, eight and ten receivers, respectively. In each case the azimuthal distribution of the stations are changed and we observe the invertibility of the G matrix by inspecting the behavior of the null vectors.

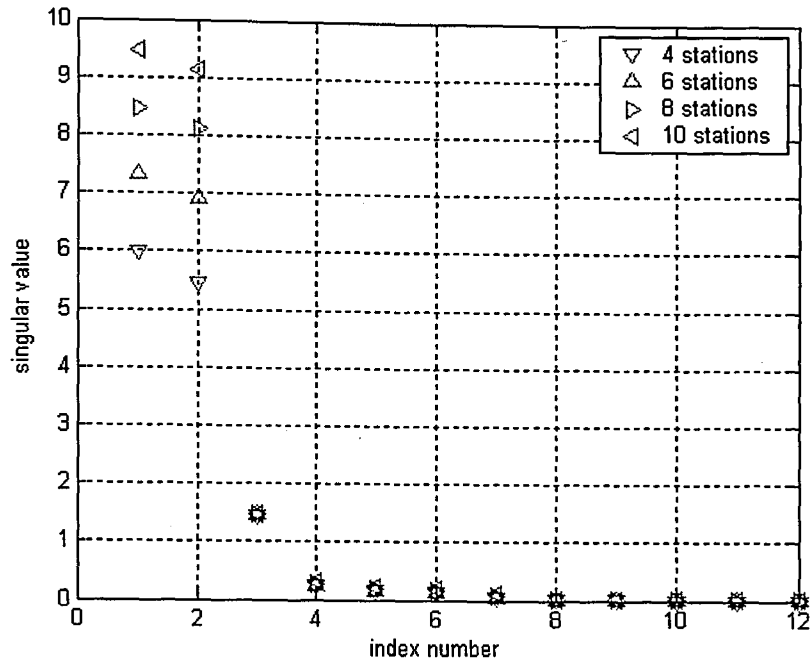

Figure 4.3 Singular values of G matrix for the first case

In the first case, the stations are located just above the hypocenters with a very small horizontal variation. With this configuration, the take-off angles are all defined as being near to values of π and the variation of the azimuth angles is assumed very small. The results are shown in Figure 4.3 where the singular values of G matrix are plotted versus the number of station used for each model. It is observed that in this experiment all of the singular values converge to zero except the first two. This means that observing all events from single location and from a narrow angle will give identical and redundant information. That will result in creating dependent linear equations in the system that in turn will result in high number of null vectors in the G matrix and will make the inversion process harder to solve. That is to say, if we have such a station distribution, we would probably not be able to solve all of the unknown model parameters efficiently.

The second case is designed as if the stations are clustered only at the two azimuths. With this aim, the take-off angles are defined with small variations around $3\pi/4$. Figure 4.4 shows the singular values of G matrix.

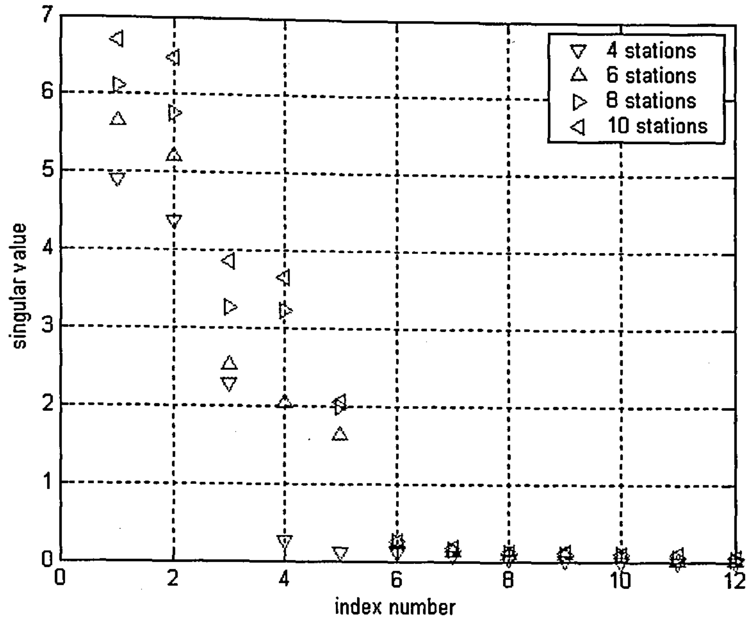

Figure 4.4. Singular values of G matrix for the second case

As can be seen in the Figure 4.4, the number of singular values converging to zero, hence the number of null vectors is reduced. This is resulting from the decrease in the number of linearly dependent equations in the linear system. That corresponds to the fact that if we observe the events from two different locations we have two sources of non-redundant types of information.

For the last step of this experiment, the azimuthal distribution of the stations is defined with a good coverage. Figure 4.5 shows the singular values of G matrix that is constructed considering good station coverage. It should be obvious that decreasing seismic gap with respect to the events contributes to the solution of the G matrix. That is to say, the station coverage is very important factor for the efficiency of double difference method.

Now we analyze the effect of the number of station in the stability of the inversion process. As seen in Figure 4.3, 4.4 and 4.5, if the number of station increases, the number of null vectors decreases which is seen by the increasing number of singular values that are closer to zero. Especially in Figure 4.5, the contribution of the number of stations to the solution is very clear since the singular values of the G matrix constructed for ten stations are clearly greater than the other singular values. Therefore, it can be argued that the number of station is also an important factor for the applicability of double difference method.

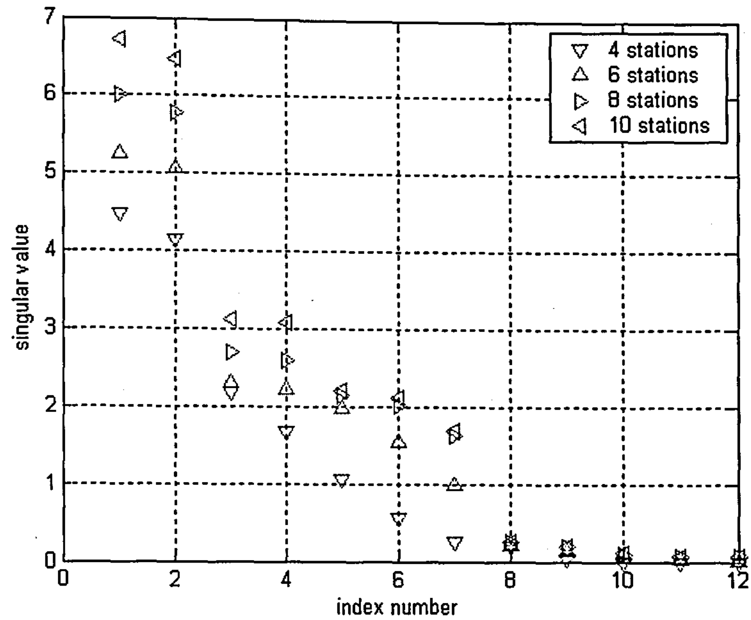

Figure 4.5 Singular values of G matrix for the last case

Throughout these experiments, we calculated the singular values of G matrices constructed with, as well as without a priori information. Without a priori information, there is at least one null vector in the G matrix. This is true even if the case of the number of rows is high to guarantee the over-determined case, and even if the rows are all linearly independent. Therefore, it should be expressed that a priori information should be imposed and be included as an extra row in the G matrix in order to deal with the nonuniqueness of the solution of the inverse problem (Waldhauser and Ellsworth , 2000).

4.2. Delay Measurement

In this part, we investigated the delay measurement methods in signal processing. There are basically two different approaches: the time domain and the frequency domain methods. The first approach, which is carried out in time domain simpler and is more suitable for automatic implementation, therefore this is the one used throughout this thesis. This method is going to be in section 4.3.1. The second method is more accurate but less practical. The second approach improves the resolution of delay measurement by using the phase information of the cross spectral density.

We have provided basic definition of both methods and performed numerical experiments using MATLAB in order to compare their performances,. This method is analyzed by numerical experiments in section 4.2.1.2. as it will be discussed in section 4.3.2.

4.2.1. Time Domain Approach: Cross-correlation

4.2.1.1 Basic Definitions

Cross correlation is used to measure the information about the relationship between two different signals. It measures both time delay and linear dependency of different time series. The delay between two signals is measured by the zero shift of the maximum value of the cross correlogram.

A typical plot of cross-correlation function is shown in Figure 4.6.b that is called cross-correlogram.

The correlation function calculates the degree of similarity between random data pairs that contains two different time series. For each time shift between the signals, a different correlation coefficient exists. The mathematical expression of correlation coefficient (r) is;

$$r = \frac{R_{xy}(0)}{\sqrt{R_{xx}(0)R_{yy}(0)}} \tag{4.26}$$

where $R_{xy}(\tau)$ is defined as:

$$R_{xy}(\tau) = \lim_{T\to\infty} \frac{1}{T}\int_0^T x(t)y(t+\tau)dt \qquad (4.27)$$

The cross correlation function in discrete time domain is described by equation

$$R_{xy}(\tau) = \sum_t x(t)y(t+\tau) \qquad (4.28)$$

It means that the correlation coefficient (r) used in statistic, corresponds to the maximum value of the normalized cross correlation function.

The sensitivity of the discrete cross correlation function is bounded by the sampling rate. In other word, it does not provide delay measurement smaller than of the sampling rate. In such a case, it is possible to measure the time delays by interpolating the data to a higher sampling rate before the cross correlation process is applied. This allows the measurement of the time differences with a better resolution.

In numerical analysis, interpolation is a method of constructing new samples from a known discrete data set. It is a kind of curve fitting method, where the function must exactly go through the known data points. In this study, we adopt spline function method for interoplating the signals. This method using natural cubic spline utilizes third-degree polynomials, which are fitting together between the known samples. The natural cubic spline is piecewise cubic and twice continously differentiable. Furthermore, its second derivative is zero at the end points.

4.2.1.2. Experiments

To start with, two exponentially decaying sine signals were constructed with sampling rate of 0.01 second. One of the signals was delayed 0.1 second from the other (Figure 4.6.a). Random noise was added to both signals. Then cross correlation function has been calculated as indicated in Figure 4.6.b. One can see that at this resolution level it is not easy to see the time shift of the main peak. We therefore enlarge (zoom) the section of the cross correlation waveform that corresponds to the main peak. The peak value of cross correlation function as zoomed in Figure 4.6.c., shows that the time shift is –0.1 second as was originally defined.

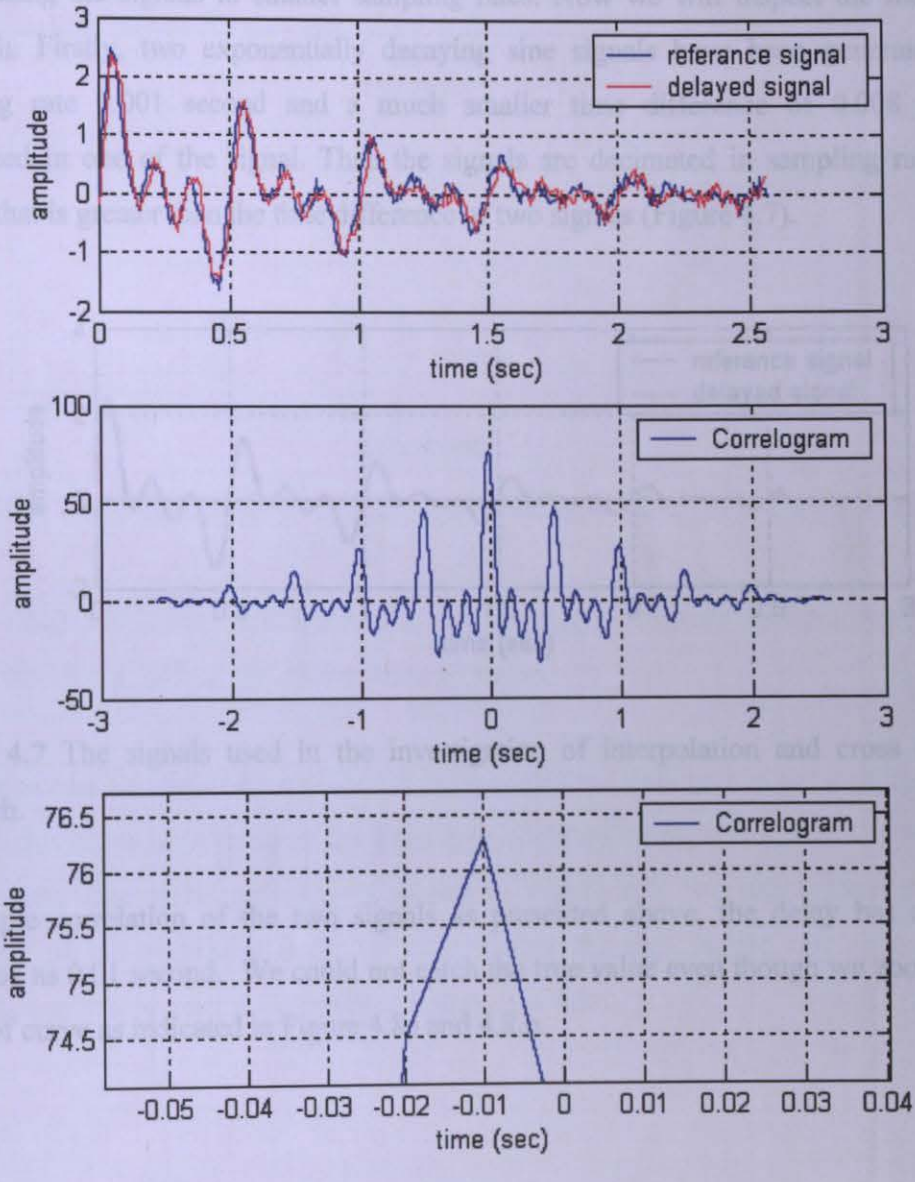

Figure 4.6 The Figures at the top are; the signals (a), the calculated correlation function (b) and the peak value of cross correlation (c).

In practice the situation may not be as simple as given above. The delay between the signals can be smaller than the sampling rate of measurement. In the studies that are interested in high resolution of delay measurements, the delays smaller than the sampling rate carry a great importance. In such cases resolution of the cross correlogram might be increased by interpolating the signals to smaller sampling rates. Now we will inspect the interpolation approach. Firstly, two exponentially decaying sine signals have been generated with a sampling rate 0.001 second and a much smaller time difference of 0.008 second is introduced in one of the signal. Then the signals are decimated in sampling rate of 0.01 second that is greater than the time difference of two signals (Figure 4.7).

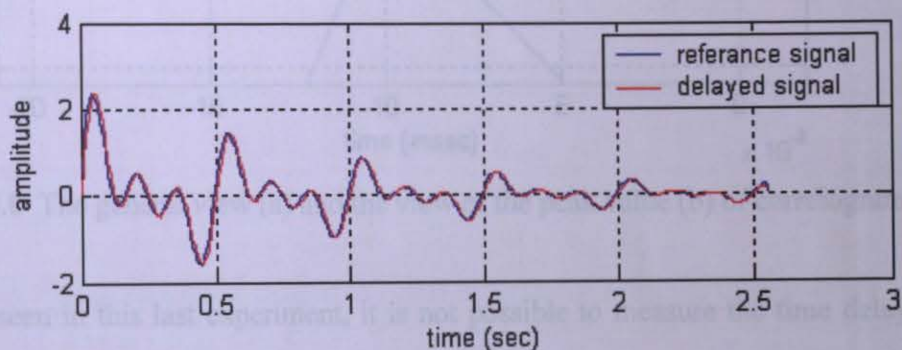

Figure 4.7 The signals used in the investigation of interpolation and cross correlation approach.

By simple correlation of the two signals as presented above, the delay has again been measured as 0.01 second. We could not catch the true value even though we zoomed in the center of curve as indicated in Figure 4.8a and 4.8.b.

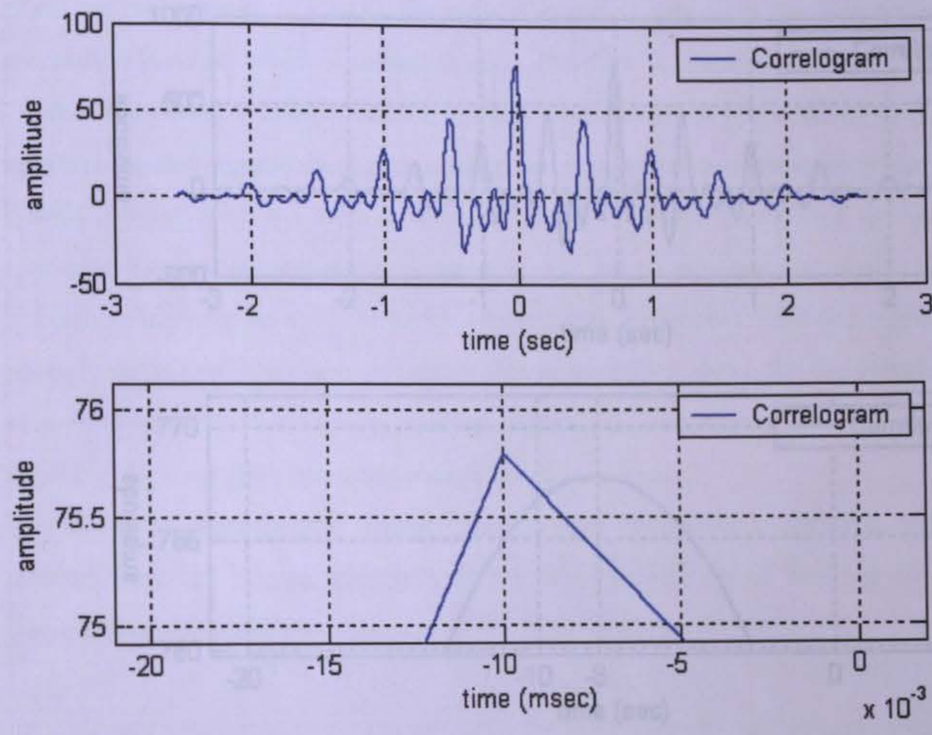

Figure 4.8 The general view (a) and the view of the peak value (b) of correlogram.

As it is seen in this last experiment, it is not possible to measure the time delay, which is smaller than the sampling rate, without interpolation.

In order to attain a higher sensitivity, we interpolated the data pair to get a higher sampling rate and this allow us to measure the finer delay time by cross correlation. The result of the improvement due to interpolation is shown in Figure 4.9. We could measure the time difference of the signals properly by interpolating the data before calculating the cross correlation as can be seen in the zoomed Figure of 4.9.b,

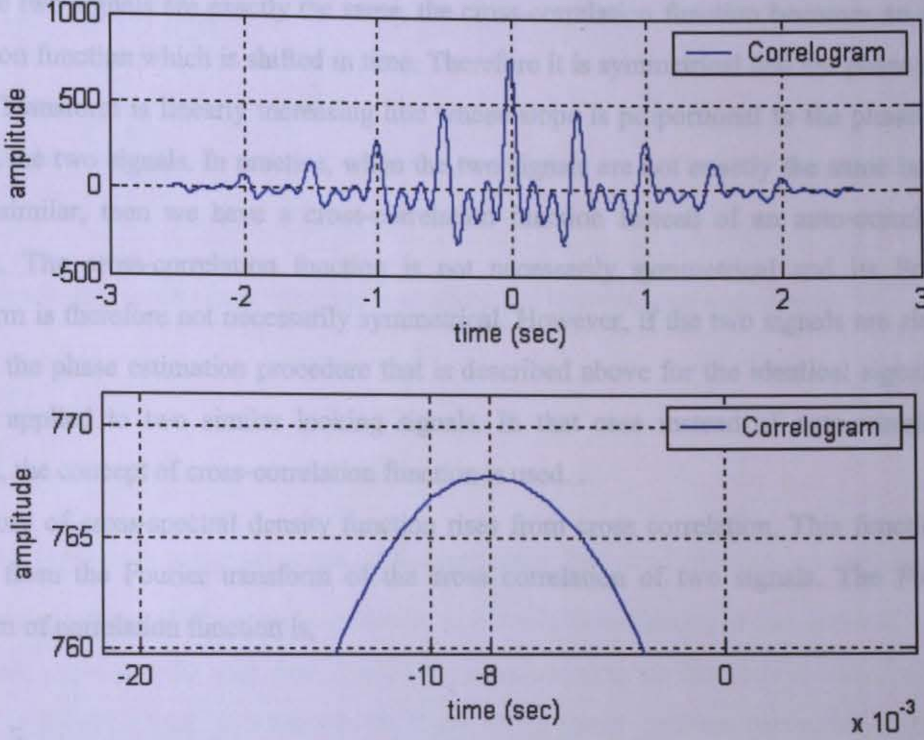

Figure 4.9 The general view (a) and the view of the peak value (b) of correlogram

We conclude that the time domain interpolation method is simple and very useful for determining the delay of signals with high resolution.

4.2.2. Frequency Domain Approach: Cross-Spectral density function

4.2.2.1 Basic Definitions

This approach is based on the fact that the Fourier Transform of a function which is symmetrical with respect to origin time t=0 (even function), has a particular form. The Fourier Transform is that case is purely real and the phase is zero for all frequencies. If the even function is shifted in time axis, in other word becomes symmetrical with respect to a time t=τ, then the phase of the Fourier Transform is a function which increases linearly with frequency and where the rate of increase is proportional to the time shift τ. This property can be used to estimate the time shift between two similar (or roughly similar) signals. The signals for which the phase difference is to be estimated are cross correlated. In ideal case, when the two signals are exactly the same, the cross-correlation function becomes an auto-correlation function which is shifted in time. Therefore it is symmetrical and the phase of its Fourier Transform is linearly increasing line whose slope is proportional to the phase shift between the two signals. In practice, when the two signals are not exactly the same but are closely similar, then we have a cross-correlation function instead of an auto-correlation function. The cross-correlation function is not necessarily symmetrical and its Fourier Transform is therefore not necessarily symmetrical. However, if the two signals are similar enough, the phase estimation procedure that is described above for the identical signal can also be applied to two similar looking signals. In that case instead of auto-correlation function, the concept of cross-correlation function is used. .

The theory of cross-spectral density function rises from cross correlation. This function is derived from the Fourier transform of the cross correlation of two signals. The Fourier transform of correlation function is,

$$S_{xy}(f) = \int_{-\infty}^{\infty} R_{xy}(\tau) e^{-j2\pi 2} d\tau \qquad (4.24)$$

Since a cross correlation function is not an even function, cross-spectral density function is mostly a complex number as,

$$G_{xy}(f) = C_{xy}(f) - jQ_{xy}(f) \qquad (4.25)$$

where the real part, C_{xy}, is called coincident spectral density function, and the imaginary part is called quadrature spectral density function. In polar notation, the cross-spectral density function is denoted as

$$G_{xy}(f) = |G_{xy}(f)| e^{-j\theta_{xy}(f)} \qquad (4.26)$$

Magnitude $|G_{xy}(f)|$ and the phase angle $\theta_{xy}(f)$ are calculated by C_{xy} and $Q_{xy}(f)$ as;

$$G_{xy}(f) = \sqrt{C^2{}_{xy}(f) + Q^2{}_{xy}(f)} \tag{4.27}$$

$$\theta_{xy}(f) = \arctan\left(\frac{C_{xy}(f)}{Q_{xy}(f)}\right) \tag{4.28}$$

For any frequency value f interested, the time delay can be calculated individually by;

$$\tau = \frac{\theta_{xy}(f)}{2\pi f} \tag{4.29}$$

where θ_{xy} represents the phase angle of the frequency interested in cross spectral density. The phase spectrum of cross spectral density is a curve that consists of the series of phase angles. We know that the shift from zero of the cross correlogram that defines the time shift between two signals leads to a trend in the shape of the phase spectrum curve. Although the phase spectrum curve is not a flat line as would be expected if two signal were identical, a straight line can be fitted to find an approximation to the case of two similar looking signals as can be seen in Figure 4.11.b. This can be approximated by fitting a line to phase curve whose slope defines the delay between signal pairs.

4.2.2.2. Experiment

For this experiment, again we constructed two exponentially decaying signals with a small sampling rate of 0.001 sec. Random noise was added to the signals. One of the signals was delayed 0.005 second from the other. After that, we have decimated signals with a sampling rate 0.01 in order to conceal the delay time at the interval of known data points. The signals are shown in Figure 4.10.

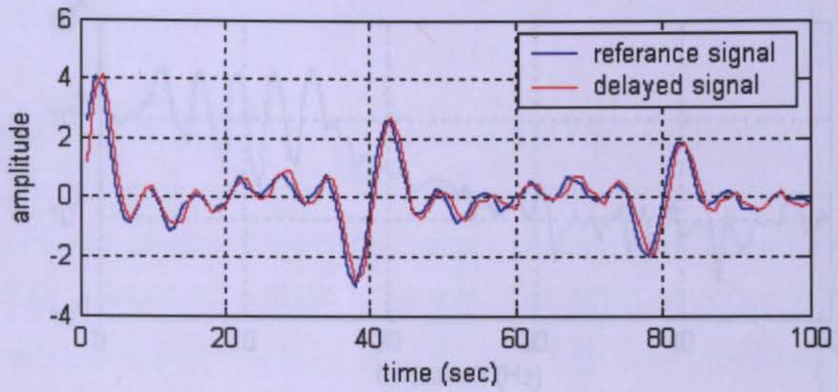

Figure 4.10. The signals used in the experiment.

We computed the cross-power density spectrum of the signals as introduced in section 4.2.2.1. We fit a line to the phase spectrum with least squares approach (Figure 4.11.a) in the 'significant part' of the frequency range (0-20 Hz in this example) which is determined by the dominant frequencies as given by the larger amplitudes of the power density spectrum (Figure 4.11.b).

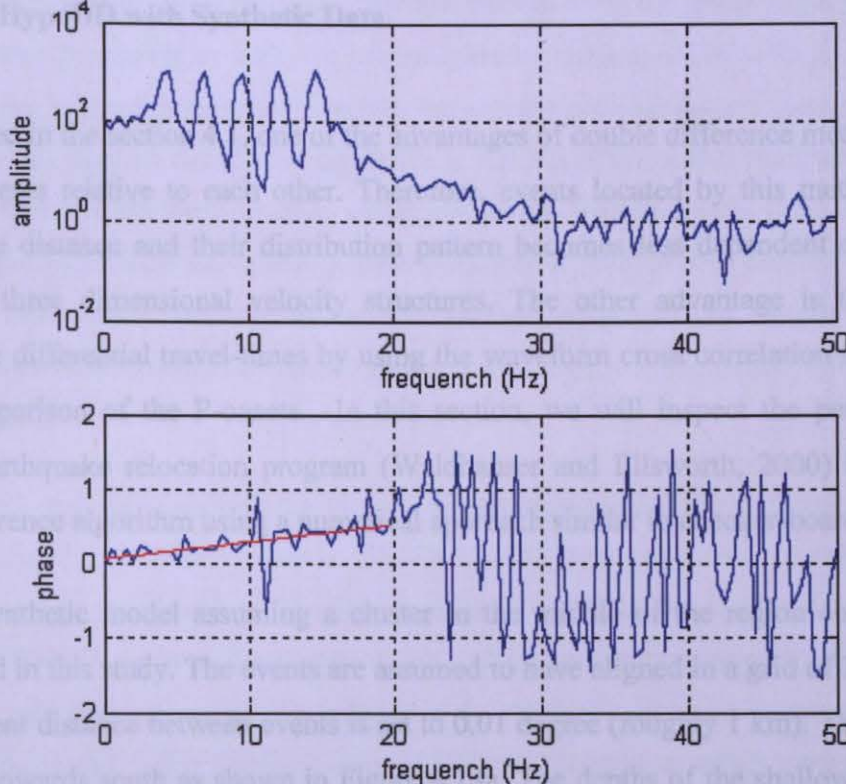

Figure 4.11. Amplitude spectrum (a) and phase spectrum (b) of cross spectral density

The slope of the fitted line is given by:

$$\tan\theta = \frac{0.0611}{19.697} = 0.0310$$

and the delay is;

$$\tau = \frac{0.0310}{2\pi} = 0.0049$$

In this experiment, the time difference between signals was estimated as 0.0049 sec, which was set to 0.005 sec at the beginning. Although the delay introduced between two signals is smaller than the sampling rate, the cross-spectral density does not need a prior interpolation process to measure the delay with the required accuracy. Considering the resolution of time delay measurement based on the frequency domain approach, this method is quite efficient to measure the delay between doublets in comparison with the time domain approach. However, this method requires off-line inspection and evaluation of phase curves therefore not applicable for large volume of dataset.

4.3 Testing HypoDD with Synthetic Data

As introduced in the section 4.1, one of the advantages of double difference method is ability to locate events relative to each other. Therefore, events located by this method preserve their relative distance and their distribution pattern becomes less dependent on the lateral changes in three dimensional velocity structures. The other advantage is the ability to calculate the differential travel-times by using the waveform cross correlation instead of the simple comparison of the P-onsets. In this section, we will inspect the performance of HypoDD earthquake relocation program (Waldhauser and Ellsworth, 2000) based on the double difference algorithm using a numerical approach similar to checker-board test.

We set a synthetic model assuming a cluster in the middle of the region covered by the stations used in this study. The events are assumed to have aligned in a grid of 10x10 events. The interevent distance between events is set to 0.01 degree (roughly 1 km). The grid has an inclination towards south as shown in Figure 4.13a. The depths of the shallower events are starting from 5 km in the north and increasing continuously to 9.5 km in the south with the increment of 0.5 km for each line of the grid. The variation of depth of the events was introduced with the purpose of comparing the solution quality of the conventional method with the double difference method with respect to all spatial 3-dimensions.

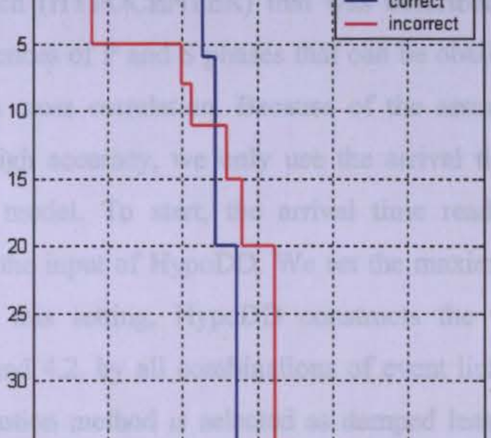

Figure 4.12 The velocity models used in synthetic test

We calculated the travel times of events for each station using the given velocity model indicated by blue lines in Figure 4.12. We assumed that this velocity model is the correct one that corresponds to the real case and therefore the arrival time readings are assumed to be exactly true. This data set constructed synthetically represents the arrival readings that are used in the routine earthquake location techniques as the data vector. In practice, when solving the inverse problem the velocity model is not well known and that prevents us from locating the earthquakes correctly. In order to perform a realistic test, we located the synthetic events using a different velocity model than the correct one which was used in forward modeling.

In Figure 4.12, red line indicates the velocity model representing the incorrect velocity structure. We used a modified version of HYPOCENTER program (Lienert and Havskov, 1995) for locating synthetic events. The hypocentral and epicentral location results obtained from HYPOCENTER program are shown in Figure 4.13.b and 4.14.b, respectively. These results are a good illustration of the dependency of the classical earthquake location methods on the velocity model. The locations estimated by the classical approach, especially the depth results are clearly scattered from the original positions. This result shows that, with the station geometry and using the conventional location procedures, the depth estimations are subject to larger error than the horizontal coordinates.

The next step is to test the performance of the double difference algorithm using the same data, ie using the same arrival times. We use the same incorrect velocity model that was used in the conventional approach (HYPOCENTER) that was described previously. HypoDD make use of the time differences of P and S phases that can be obtained from either arrival time readings or waveform cross correlation. Because of the assumption that the arrival readings are picked with high accuracy, we only use the arrival time readings that were calculated in the forward model. To start, the arrival time readings are converted to differential travel times for the input of HypoDD. We set the maximum interevent distance parameter to 3 km. With this setting, HypoDD constructs the G matrix, which was introduced in sections 4.1 and 4.2, by all combinations of event links having distance less than 3 km. The inverse solution method is selected as damped least square with damping factor of 70 that are set using ISOLV and DAMP parameters in HypoDD program.

The hypocentral and epicentral relocation results obtained from HypoDD program in are shown in Figure 4.13.c and 4.14.c, respectively. Inspecting the relocation results, we see that distribution geometry is closer to the original one in the double difference approach as compared to the classical one. The epicentral distribution of events relocated by HypoDD exhibits a geometry that is even more compatible with the original epicentral locations. However, the hypocenters of relocated earthquakes, especially the depth estimations, also deviate from the original hypocenters but to a lesser degree as seen in Figures 4.13.a and 4.13.c.

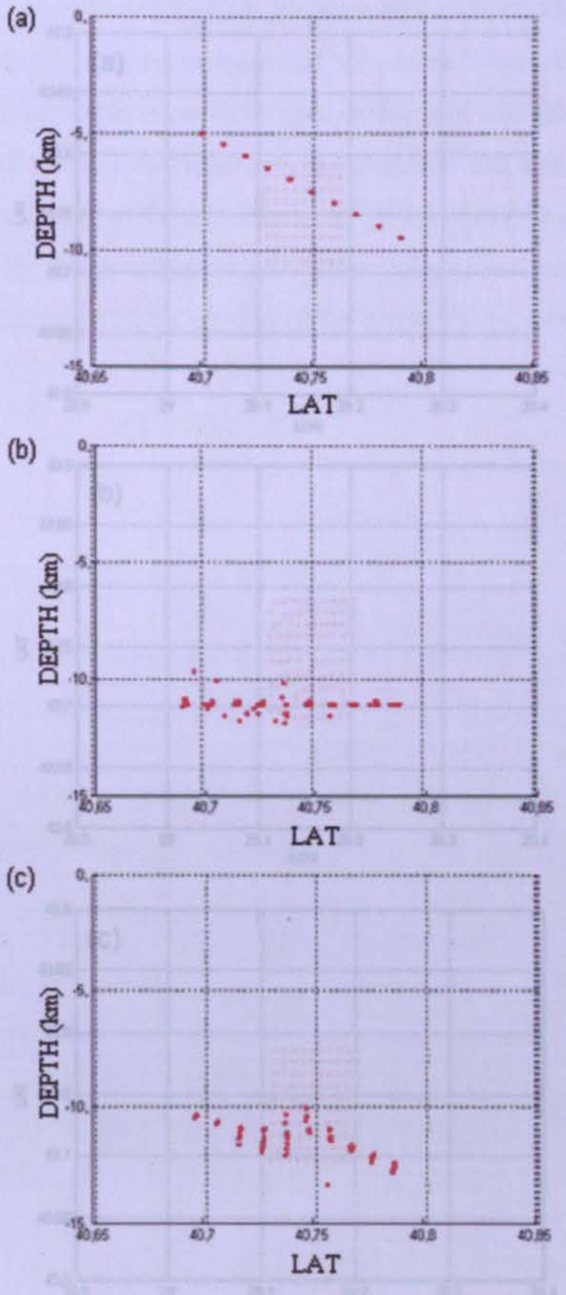

Figure 4.13 (a) Depth sections of the original events, (b) the events located by HYPOCENTER and (c) the events relocated by HypoDD. Note the improvement brought by HypoDD.

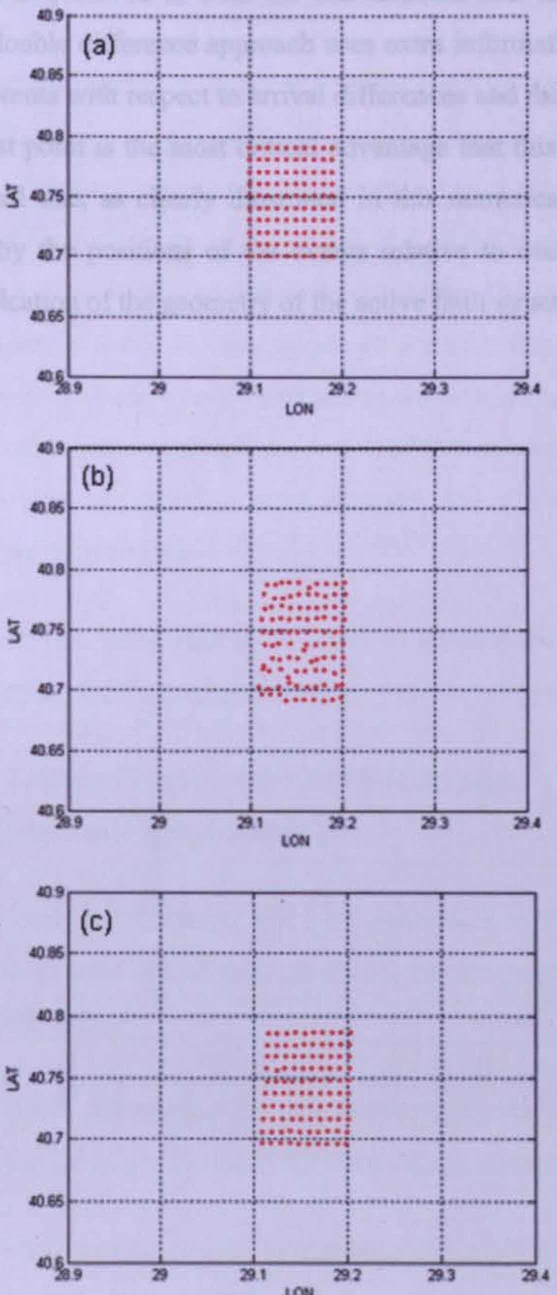

Figure 4.14 Epicenters of the original events (a), the events located by HYPOCENTER (b) and the events relocated by HYPODD (c)

It can be seen clearly that the centroid of the cluster containing the estimations of earthquake locations are shifted to south-east in both Figure 4.14.b and Figure 4.14.c relative to the original one in Figure 4.14.a. If the average velocity model deviates from the true one, and if the stations are distributed unevenly, the located events are subject to a translation horizontally. This effect is observed in both the conventional and the double difference approach. However, the double difference approach uses extra information. It optimizes the relative positions of the events with respect to arrival differences and therefore preserves the cluster geometry. This last point is the most critical advantage that this method offers with respect to the conventional one, as clearly illustrated in this numerical experiment. This extra information given by the positions of the events relative to each other, contributes significantly to the identification of the geometry of the active fault structures.

5. RELOCATION OBTAINED BY DOUBLE DIFFERENCE METHOD

The main purpose of this study is to revise a part of the aftershock locations of the 17 August 1999 Izmit Earthquake (Karabulut et al, 2002). We decided to use the double difference (DD) method in order to improve the location of the earthquakes. As introduced in Chapter 4, double difference algorithm utilizes the differential travel times of event pairs. This data set can be prepared by using either the arrival time readings directly from the catalog or the use of the cross correlations of S and P phase windows for improving the accuracy. The former database is quite easy to obtain by only subtracting the selected arrival times from the hypo-input file used in routine location algorithms (i.e. HYPO71 locating program, Lee and Lahr, 1975). The second approach, which is more accurate, requires delay estimations by methods described in the previous chapter.

We first constructed a software infrastructure in order to prepare the inputs of HypoDD automatically. For that purpose 4 different software tools were developed:

1- changesac.csh: This is combined C-shell scripts and SAC macros. It is used for changing the name of the events in accordance with the event IDs.

2- dtcc.csh: This is combined C-shell scripts and SAC macros. It executes the second and most critical step which is to correlate all the waveforms for the possible event pairs and eventually find the time differences.

3- dtccfilter.m: This is a MATLAB routine. It executes the third critical step that eliminates the event pairs with low correlation coefficient (<0.5) from the waveform based catalog,

4- dt.ct.filter.csh: This C-shell routine is used to eliminate the event pairs appearing in the waveform based catalog, from the arrival based catalog.

The data set was collected from a temporary network located around the Çınarcık Basin and Izmit Bay (Karabulut et al, 2002). The network was installed ten days after the main shock of 17 August 1999 Izmit earthquake. Additional data set was obtained from the other seismic network operated by TUBITAK Marmara Research Center for a better station distribution. The station distribution is shown in Figure 5.1.

The data set allowed us to use both of the delay measurement methods for double difference algorithm.

We know that each event cluster might differ from each other on their data properties because of different network geometries. Different data properties lead the event clusters to have individual parameter sensitivities to the inversion processes. For this reason, the seismicity was analyzed in classifying the total event sequence into three main clusters, namely Tuzla, Yalova and Central clusters as shown in Figure 5.1.

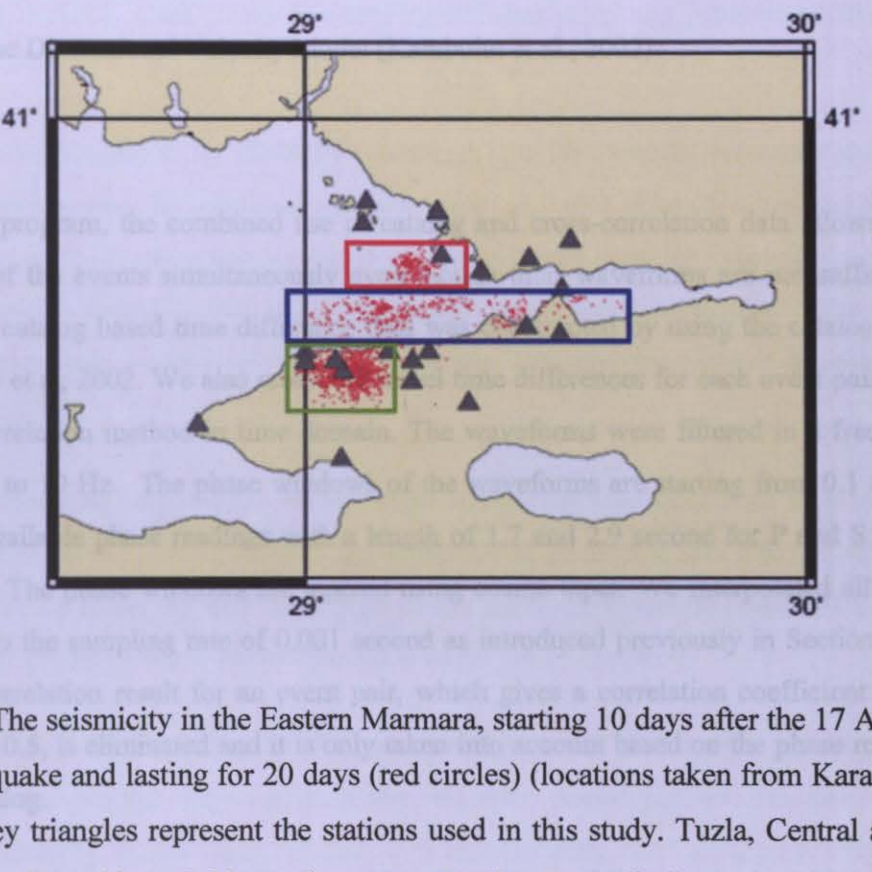

Figure 5.1 The seismicity in the Eastern Marmara, starting 10 days after the 17 August 1999 Izmit Earthquake and lasting for 20 days (red circles) (locations taken from Karabulut et al., (2002)). Grey triangles represent the stations used in this study. Tuzla, Central and Yalova clusters are indicated by red, blue and green rectangles, respectively.

More than 2500 events have been detected by at least three stations by Karabulut et al. (2002). The events were selected according to the relative horizontal and vertical uncertainties of location estimations, which are less than 2 km and 3 km, respectively. We relocated 1598 of these events using a 1-D velocity model obtained by Karabulut et al, (2002) using VELEST (Kissling et al., 1994) approach (Table 5.1). The combinations of the event pairs for HypoDD were determined considering the maximum hypocentral separation distance (MAXSEP) to be 4.0 km.

Depth, km	V_p (km sec^{-1})	V_S, (km sec^{-1})
0.00	2.25	1.10
1.00	5.70	3.20
6.00	6.10	3.60
20.00	6.80	3.85
33.00	8.00	4.55

Table 5.1 One Dimensional Velocity Model (Karabulut et al., 2002)

In HypoDD program, the combined use of catalog and cross-correlation data allows us to relocate all of the events simultaneously even though their waveforms are not sufficiently similar. The catalog based time difference data was constructed by using the catalog given by Karabulut et al, 2002. We also measured travel time differences for each event pair using the cross correlation method in time domain. The waveforms were filtered in a frequency band from 2 to 10 Hz. The phase windows of the waveforms are starting from 0.1 second before the available phase readings with a length of 1.7 and 2.9 second for P and S phase, respectively. The phase windows are tapered using cosine taper. We interpolated all of the waveforms to the sampling rate of 0.001 second as introduced previously in Section 4.2.1. The cross-correlation result for an event pair, which gives a correlation coefficient that is smaller than 0.5, is eliminated and it is only taken into account based on the phase readings from the catalog.

We used damped least square method to solve the system of linear equations because the singular value decomposition is found to be computationally difficult for solving large and ill-conditioned systems (Waldhauser, 2000).

The contribution of the data vector to the solution is first determined according to the quality factor for each event pair that can be obtained from the pick quality factor for the catalog data and the value of the correlation coefficient for the cross correlation data .The resolution of the quality indicator of catalog data is dramatically lower because it can only have the values of 1, 0.75, 0.5 and 0.25, in comparison with the weights of cross correlation data which varies continuously between 1-0.5. HypoDD enables us to apply another weighting factor by settings of WTCCP, WTCCS (Weight for cross-correlation data of P-wave and S-wave), WTCTP and WTCTS (Weight for catalog data of P-wave and S-wave), defining the contributions of entire catalog and cross correlation data sets to the solution of inverse problem. In this study, we set WTCCP and WTCCS to relatively greater values than the WTCTP and WTCTS. Each cluster has slightly different weighting parameters from each other.

In HypoDD, the damping factor (DAMP) determines how fast the solution converges. Large damping factors prevent the solution from converging, so it also affects the iteration number (NITER). We set the iteration numbers in accordance with the damping factor. The optimum damping factor is selected by trial and error considering the condition number of the system (CND) and root mean square (rms) residual reduction. The condition number is supposed to be smaller than 100.

During the iterations, some of the events might completely lose their links as a result of iteration processes. In addition, some of the events might be located above the ground after relocation. In such cases, HypoDD take these events out of the inversion process. Therefore, the number of events before and after relocation might not be the same.

With the purpose of visualizing the 3-dimentional character of the seismic activity, we inspected all the possible view-angles of the relocation results in three dimension using Matlab. Additionally, we also took parallel depth sections using GMT in order to exhibit the consistency of the relocation results in the determined directions.

5.1 Tuzla Cluster

Firstly, we will handle the Tuzla cluster containing 210 events located on the northern edge of the Çınarcık Basin. We correlated more than 32000 waveforms for 3660 event pair combinations whose interevent distance is smaller than 4 km. We found more than 10000 good correlated waveforms (correlation coefficient > 0.5), but we used 7362 of the cross correlation observations because of the requirement that event pairs should be commonly recorded by at least three station. We eliminated the corresponding cross correlation observations from the catalog data set, thus we used 21477 catalog observations for this cluster. The parameters of WTCCP, WTCCS, WTCTP and WTCTS are set to 1.0, 0.5, 0.25 and 0.15, respectively. We defined relatively small damping factor 45 for the convergence of the solution. We set the event separation distance to 2.3 km for cross correlation and 3.0 km for catalog observations. The solution was converged sufficiently at the 20th iteration. The number of events decreased to 192 after the relocation process. In Figure 5.1, we plot the epicentral locations and general depth sections of the hypocenters given by Karabulut et al, 2002 and relocation results of HypoDD for Tuzla Cluster.

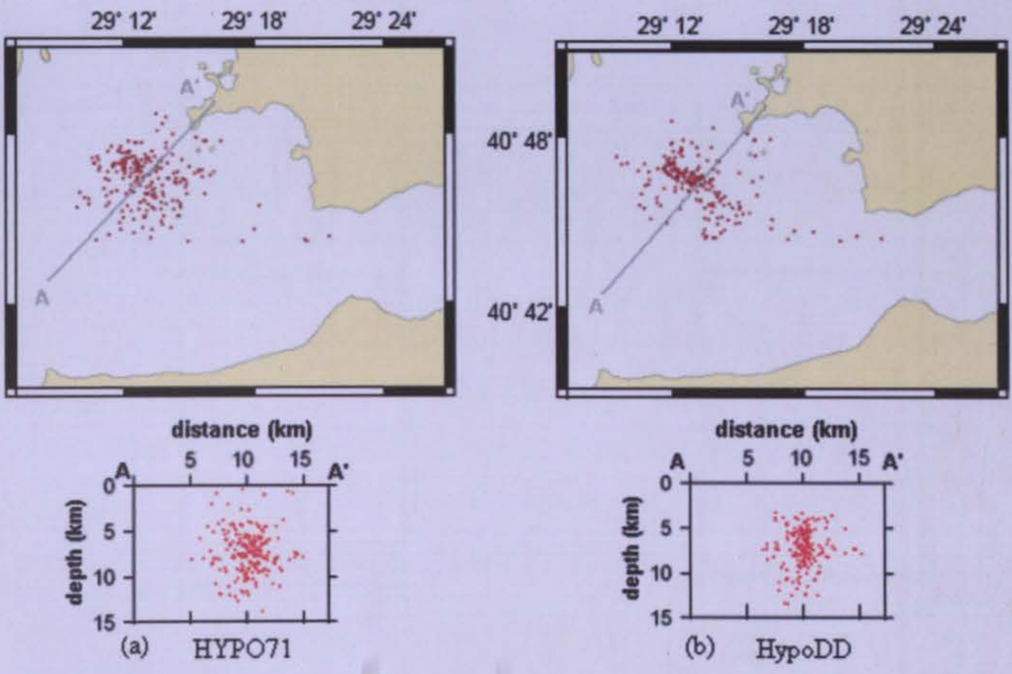

Figure 5.2 For Tuzla cluster, the epicentral locations and depth view of (a) the hypocenters given by Karabulut et al, 2002 and (b) relocation results

As can be seen in the Figure 5.1, the initial distribution of the events shows a scattered view, whereas the distribution of the relocated events shows a relatively linear trend lying from the northwest to the southeast. The depth section consists of all the events, which reflects the general characteristics of the seismic activity with depth. In Figure 5.3, we plot different depth sections that are selected perpendicular to the linear trend of the cluster in order to catch all of the details along the activity. The profiles taken, represents that the depth sections following one after another clearly consistent with each other. As a conclusion, we can say that HypoDD method dramatically improves the event locations estimated by routine analysis methods.

In this cluster, relocation results represent seismicity that is roughly dipping vertically. The seismic activity occurs between 1 and 14 km, but its dominant range is between the 4 and 12 km. The depths continuously increase along the activity from the southeast to the northwest. All of the relocation results mentioned above provide a clear geometry at depth as well as at the surface of Tuzla cluster.

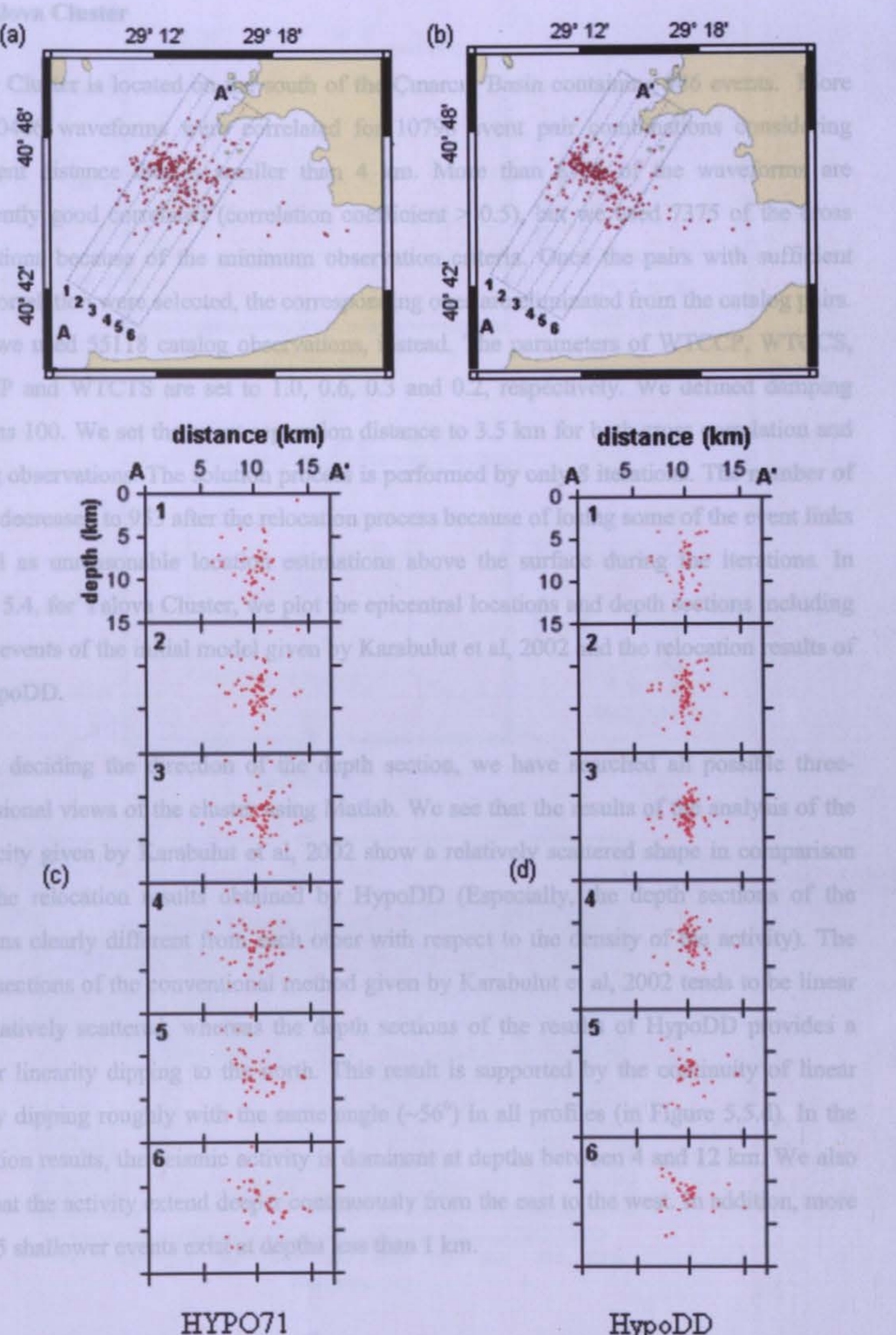

Figure 5.3 The epicentral location and detailed depth section of (a and c) the hypocenters given by Karabulut et al, 2002 and (b and d) relocation results

5.2. Yalova Cluster

Yalova Cluster is located on the south of the Çınarcık Basin containing 986 events. More than 70466 waveforms were correlated for 10796 event pair combinations considering interevent distance that is smaller than 4 km. More than 8181 of the waveforms are sufficiently good correlated (correlation coefficient > 0.5), but we used 7375 of the cross correlations because of the minimum observation criteria. Once the pairs with sufficient cross correlation were selected, the corresponding ones are eliminated from the catalog pairs. Thus, we used 55118 catalog observations, instead. The parameters of WTCCP, WTCCS, WTCTP and WTCTS are set to 1.0, 0.6, 0.3 and 0.2, respectively. We defined damping factor as 100. We set the event separation distance to 3.5 km for both cross correlation and catalog observations. The solution process is performed by only 8 iterations. The number of events decreased to 953 after the relocation process because of losing some of the event links as well as unreasonable location estimations above the surface during the iterations. In Figure 5.4, for Yalova Cluster, we plot the epicentral locations and depth sections including all the events of the initial model given by Karabulut et al, 2002 and the relocation results of the HypoDD.

Before deciding the direction of the depth section, we have searched all possible three-dimensional views of the cluster using Matlab. We see that the results of the analysis of the seismicity given by Karabulut et al, 2002 show a relatively scattered shape in comparison with the relocation results obtained by HypoDD (Especially, the depth sections of the locations clearly different from each other with respect to the density of the activity). The depth sections of the conventional method given by Karabulut et al, 2002 tends to be linear but relatively scattered, whereas the depth sections of the results of HypoDD provides a sharper linearity dipping to the north. This result is supported by the continuity of linear activity dipping roughly with the same angle (~56^{o}) in all profiles (in Figure 5.5.d). In the relocation results, the seismic activity is dominant at depths between 4 and 12 km. We also note that the activity extend deeper continuously from the east to the west. In addition, more than 75 shallower events exist at depths less than 1 km.

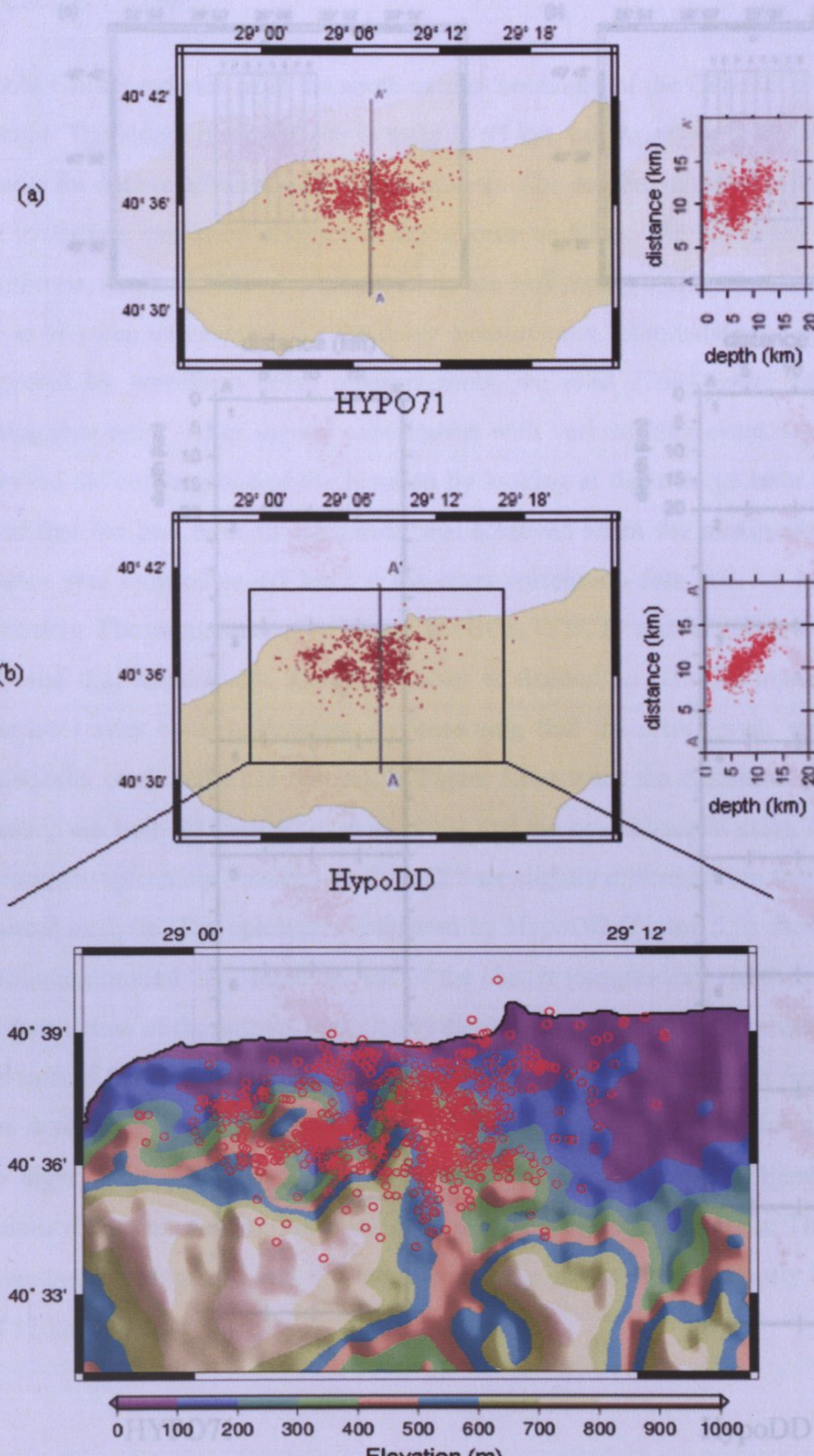

Figure 5.4 For Yalova cluster, the epicentral locations and depth views of (a) the hypocenters given by Karabulut et al, 2002, (b) relocation results (c) and relocation results on topographic map

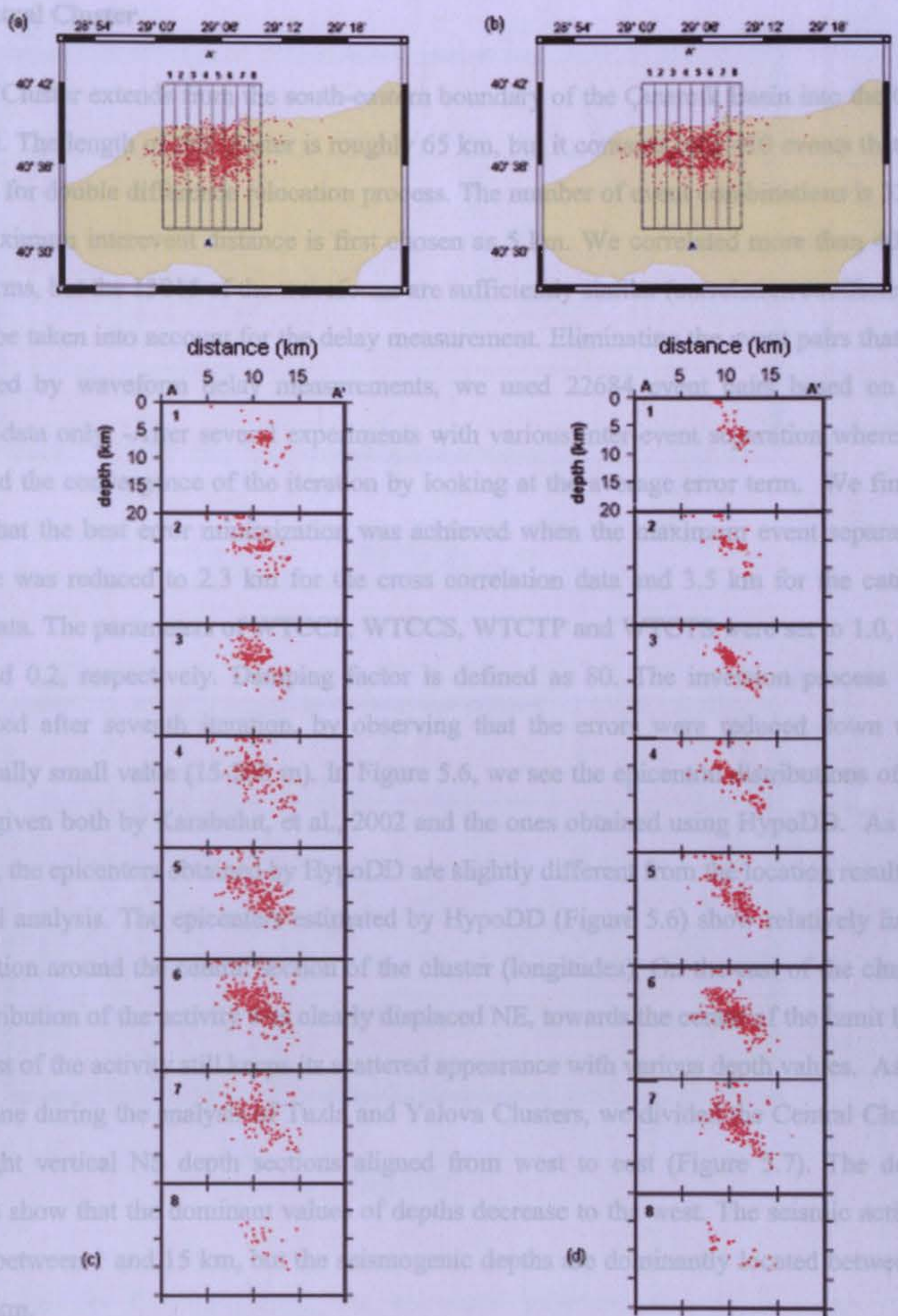

HYPO71 HypoDD

Figure 5.5 The epicentral location and detailed depth section of (a and c) the hypocenters given by Karabulut et al, 2002 and (b and d) relocation results

5.3 Central Cluster

Central Cluster extends from the south-eastern boundary of the Çınarcık Basin into the Gulf of Izmit. The length of this cluster is roughly 65 km, but it contains only 410 events that are suitable for double difference relocation process. The number of event combinations is 3251. The maximum interevent distance is first chosen as 5 km. We correlated more than 40000 waveforms, but the 13015 of the waveforms are sufficiently similar (correlation coefficient > 0.5) to be taken into account for the delay measurement. Eliminating the event pairs that are supported by waveform delay measurements, we used 22684 event pairs based on the catalog data only. -After several experiments with various inter-event separation where we observed the convergence of the iteration by looking at the average error term. We finally found that the best error minimization was achieved when the maximum event separation distance was reduced to 2.3 km for the cross correlation data and 3.5 km for the catalog based data. The parameters of WTCCP, WTCCS, WTCTP and WTCTS were set to 1.0, 0.6, 0.35 and 0.2, respectively. Damping factor is defined as 80. The inversion process was completed after seventh iteration, by observing that the errors were reduced down to a realistically small value (15-200 m). In Figure 5.6, we see the epicentral distributions of the events given both by Karabulut, et al., 2002 and the ones obtained using HypoDD. As can be seen, the epicenters obtained by HypoDD are slightly different from the location results of classical analysis. The epicenters estimated by HypoDD (Figure 5.6) show relatively linear distribution around the central section of the cluster (longitudes). On the east of the cluster, the distribution of the activity was clearly displaced NE, towards the center of the İzmit Bay. The west of the activity still keeps its scattered appearance with various depth values. As we have done during the analysis of Tuzla and Yalova Clusters, we divided the Central Cluster into eight vertical NS depth sections aligned from west to east (Figure 5.7). The depth sections show that the dominant values of depths decrease to the west. The seismic activity occurs between 1 and 15 km, but the seismogenic depths are dominantly located between 8 and 11 km.

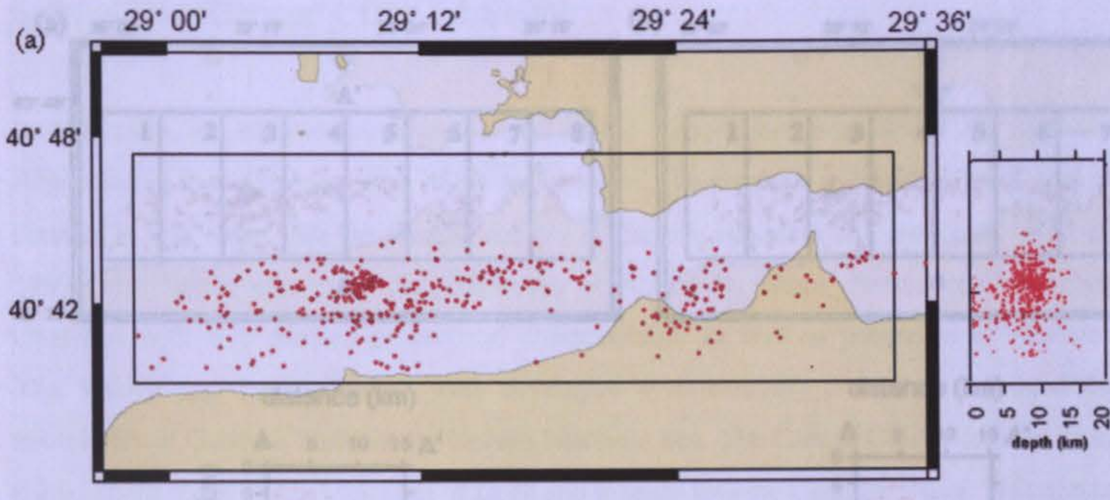

HYPO71

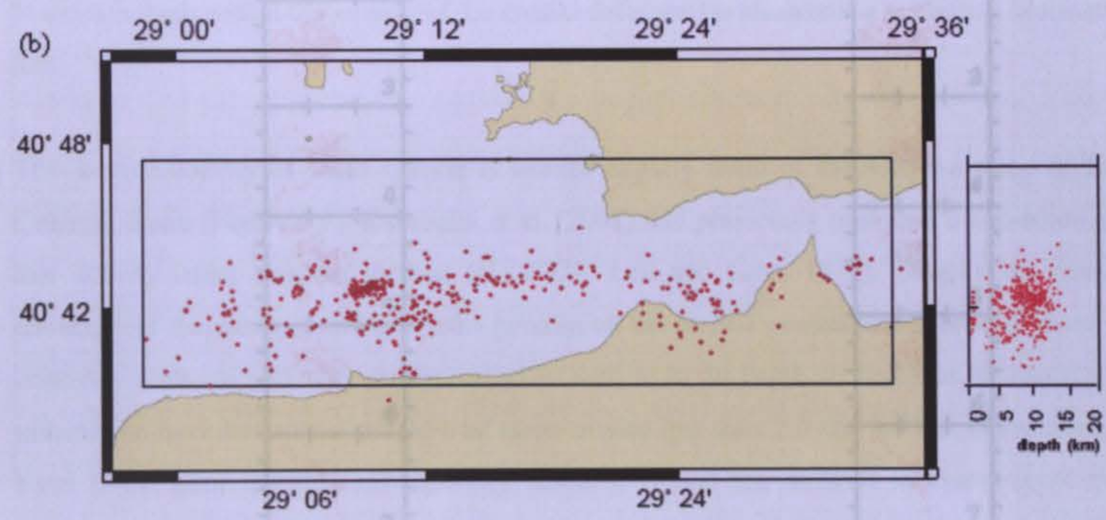

HypoDD

Figure 5.6 For Central cluster, the epicentral locations and depth views of (a) the hypocenters given by Karabulut et al, 2002 and (b) relocation results

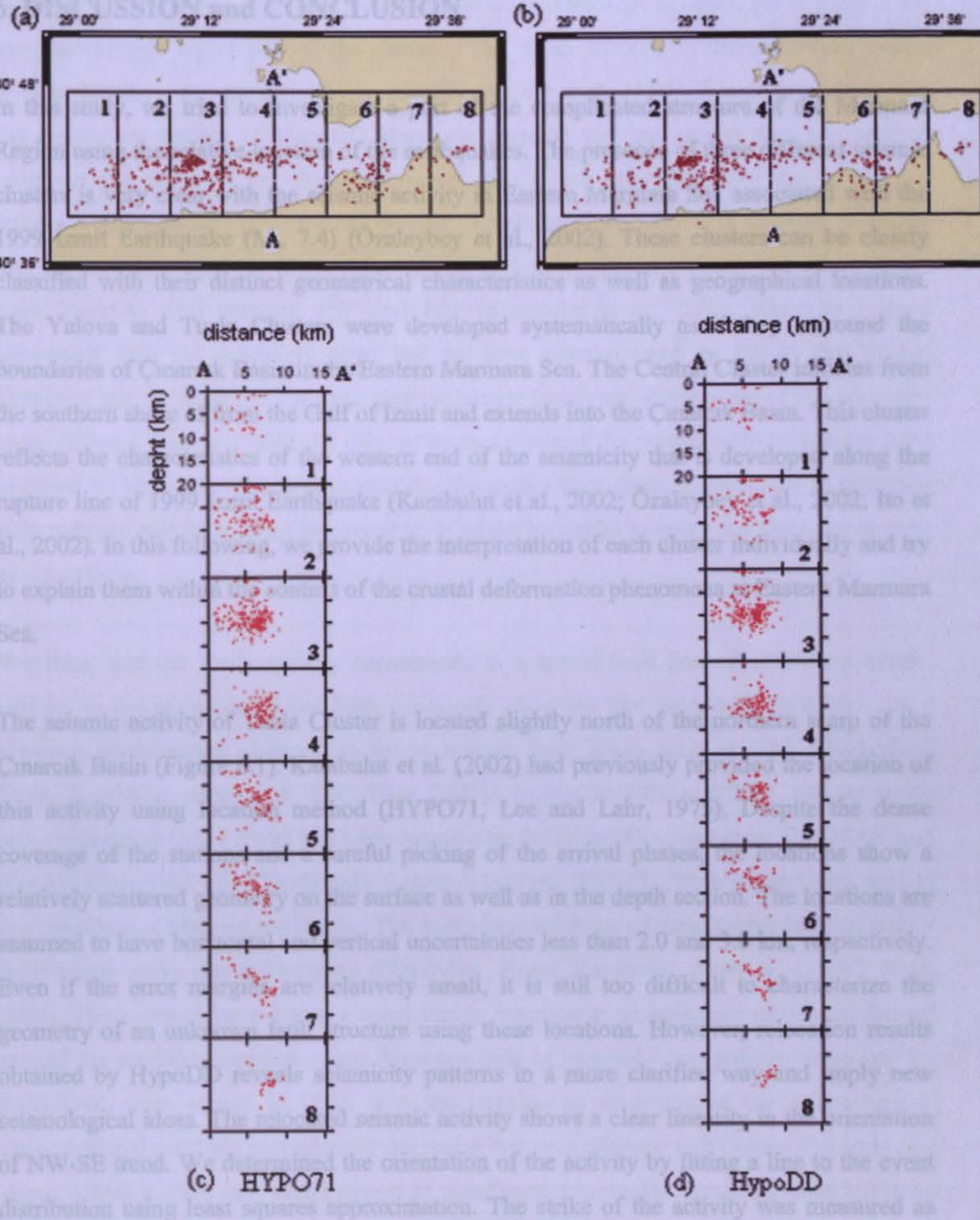

Figure 5.7 For Central cluster, the epicentral locations and detailed depth section of (a and c) the hypocenters given by Karabulut et al. 2002 and (b and d) relocation results

6. DISCUSSION and CONCLUSION

In this study, we tried to investigate a part of the complicated structure of the Marmara Region using the relative location of the earthquakes. The presence of three different seismic clusters is very clear with the seismic activity in Eastern Marmara Sea associated with the 1999 İzmit Earthquake (M_w 7.4) (Özalaybey et al., 2002). These clusters can be clearly classified with their distinct geometrical characteristics as well as geographical locations. The Yalova and Tuzla Clusters were developed systematically as if they surround the boundaries of Çınarcık Basin in the Eastern Marmara Sea. The Central Cluster initiates from the southern shore of from the Gulf of İzmit and extends into the Çınarcık Basin. This cluster reflects the characteristics of the western end of the seismicity that is developed along the rupture line of 1999 İzmit Earthquake (Karabulut et al., 2002; Özalaybey et al., 2002; Ito et al., 2002). In this following, we provide the interpretation of each cluster individually and try to explain them within the context of the crustal deformation phenomena at Eastern Marmara Sea.

The seismic activity of Tuzla Cluster is located slightly north of the northern scarp of the Çınarcık Basin (Figure 6.1). Karabulut et al. (2002) had previously provided the location of this activity using location method (HYPO71, Lee and Lahr, 1975). Despite the dense coverage of the stations and a careful picking of the arrival phases, the locations show a relatively scattered geometry on the surface as well as in the depth section. The locations are assumed to have horizontal and vertical uncertainties less than 2.0 and 3.0 km, respectively. Even if the error margins are relatively small, it is still too difficult to characterize the geometry of an unknown fault structure using these locations. However, relocation results obtained by HypoDD reveals seismicity patterns in a more clarified way and imply new seismological ideas. The relocated seismic activity shows a clear linearity in the orientation of NW-SE trend. We determined the orientation of the activity by fitting a line to the event distribution using least squares approximation. The strike of the activity was measured as 157°E. This trend is also orientated roughly parallel to the Main Marmara Fault (Le Pichon et al., 2001). The length of the activity is 25 km taking into account the scattered events extending into the Gulf of İzmit in the east. However, the densely active part of the cluster is limited to about 11 km. The activity also shows a good linearity in depth, particularly at the most seismically active part of the cluster. The depth sections of the relocation results (Figure 5.2) show that the activity dips roughly with the angle of 90°. We do not expect that the results are artifact of HypoDD since our forward test has shown that this method preserves the shape of the cluster. However, this is not consistent with the fault plane solutions which mostly gave normal faulting (Karabulut et al., 2002). In general, vertically dipping activity is likely to imply the existence of a strike slip fault plane. The strike angles were found to vary between 133° and 190° (Karabulut et al., 2002), which is a good agreement with the seismicity trend that we have approximated by LSQR line fitting. However, the dip angles of the fault plane solutions which are of the order of 70° are much more different from the vertically dipping characteristic of the seismic activity that we have obtained by HypoDD. We do not claim that the earlier fault plane solutions are in error, we only indicate that there is an incoherency. It might be useful to solve the fault planes with new locations.

We think that the Tuzla activity corresponds to a minor fault line of secondary nature, parallel to the main one. It has been previously observed that secondary fault lines are a common phenomenon observed in major seismic fault zones such as NAF (Özalaybey, Ergin, Karabulut, Aktar et al, ESC, Nice, 2003). In fact, in 2000 and 2001, two moderate size earthquakes (M_b 4.2 and 3.8) were detected by the networks operated by TUBITAK and Kandilli Observatory and Earthquake Research Institute (KOERI), both located very near to the coastlines of Maltepe and Tuzla. The fault plane solutions of these events indicate purely right lateral strike slip mechanisms (Özalaybey, Ergin, Karabulut, Aktar et al, ESC, Nice, 2003). These events have drawn a considerable attention to an existence of seismic hazard around the southern coastline of the Anatolian side of Istanbul. Two projects supported by TUBITAK were started in 2003 with the purpose of investigating the seismological, geological and geodesic properties of the region between Maltepe and Gebze. This example shows a well studied case where events of significant magnitudes should be expected away from the main fault line.

The second example of such an auxiliary deformation zone comes from a region nearer to the nucleation center of the 1999 Izmit Earthquake. Özalaybey et al. (2002) show that the largest and deepest strike-slip (30.100°E, 40.747°N, ML 6.2, depth 17 km) aftershock of the 1999 Izmit Earthquake is located not on the main rupture itself but further north (about 2 km) than the fault line (29.967°E, 40.729°N, M_w 7.4, depth 13 km) . This observation implies that rupture zones created by large earthquakes may have secondary faulting structures that might cause strong seismic events.

In Tuzla cluster, the depths of the relocated events dominantly change between 4 and 12 km, which largely coincides with the seismogenic zone in the Marmara Sea (Aktar et al., 2004). As a conclusion, we propose that the activity of Tuzla Cluster is likely to be a secondary faulting zone formed parallel to the branch of the active Main Marmara Fault (Le Pichon et al., 2001), which is located on the northern boundary of the Çınarcık Basin. The already existing faults located away from the main rupture zone are likely to have been triggered by the extensive stress that is transferred following the mainshock. Nevertheless, the activity of Tuzla Cluster should be taken into account for the presence of a seismic hazard potential near the Anatolian coastline of Istanbul.

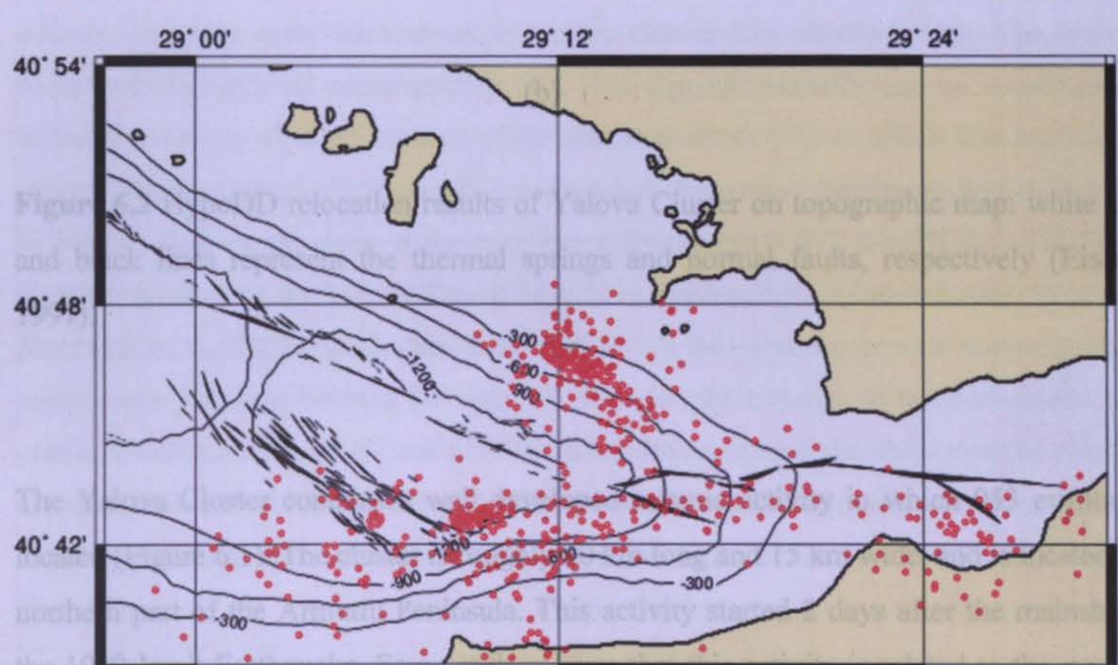

Figure 6.1 HypoDD relocation results of Tuzla and Central Clusters on bathymetric map. Fault lines are taken from Le Pichon et al., 2001.

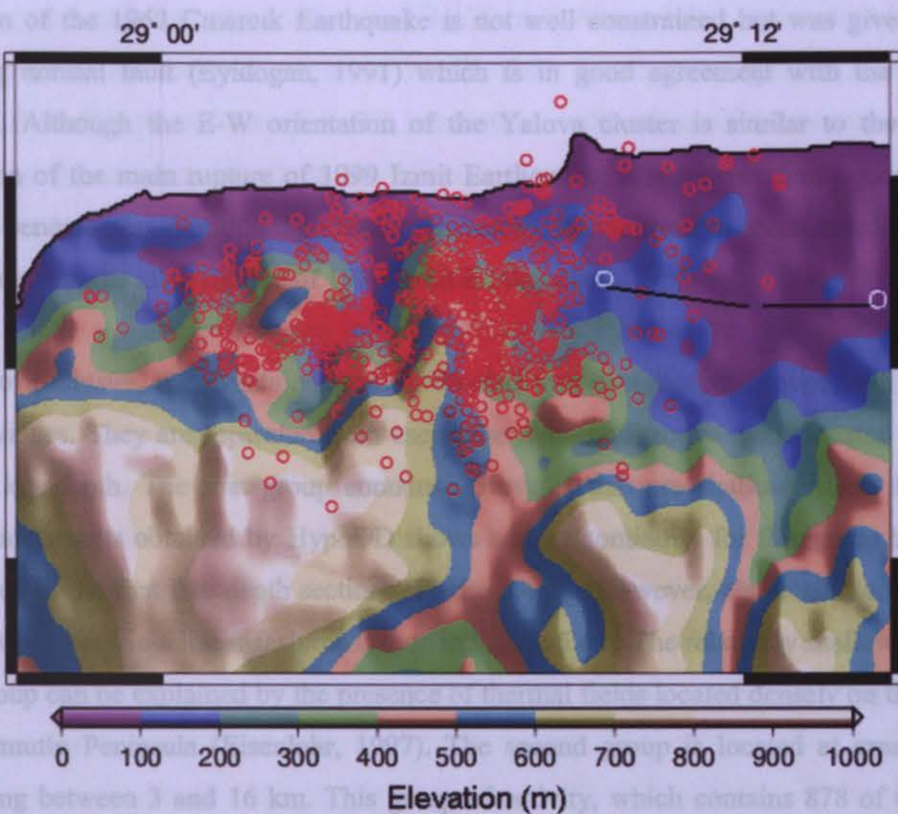

(b)

Figure 6.2 HypoDD relocation results of Yalova Cluster on topographic map: white circles and black lines represent the thermal springs and normal faults, respectively (Eisenlohr, 1997).

The Yalova Cluster contains a well developed seismic activity in which 953 events are located (Figure 6.1). The cluster is roughly 20 km long and 15 km wide, and is located in the northern part of the Armutlu Peninsula. This activity started 2 days after the mainshock of the 1999 Izmit Earthquake. Some authors state that this activity is related to the rupture of 1963 Mw 6.3 Çınarcık Earthquake (Pınar et al., 2001). This activity was also interpreted as being a late aftershock sequence of the 1963 Çınarcık Earthquake (Gurbuz et al., 2000). However, this hypothesis can not be tested fully because the exact location of the Çınarcık Earthquake is still a matter of debate. On the other hand, the estimation of fault plane solution of the 1963 Çınarcık Earthquake is not well constrained but was given as north dipping normal fault (Eyidogan, 1991) which is in good agreement with the seismicity pattern. Although the E-W orientation of the Yalova cluster is similar to the extension direction of the main rupture of 1999 Izmit Earthquake, it is independently located in the south, beneath the Armutlu Peninsula. Therefore, this cluster is considered a segment different from the main rupture of 1999 İzmit Earthquake.

In Yalova Cluster, the events are strictly divided into two distinct groups with respect to depth values. They are separated from each other with an inactive zone located between 1 and 3 km depth. The first group contains 75 events that are shallower than 1 km. The relocation results obtained by HypoDD shows a clear continuity for this group that can be observed in the first five depth sections (Figure 5.4.d). However, classically located events can not be traced in a linear fashion as seen in Figure 5.4.b. The relatively shallow activity of this group can be explained by the presence of thermal fields located densely on the north of the Armutlu Peninsula (Eisenlohr, 1997). The second group is located at greater depths changing between 3 and 16 km. This group of activity, which contains 878 of the events, reflects clearly the main characteristic of Yalova Cluster. The activity linearly dips to the north with an angle of approximately 56°. This dipping geometry can be consistently followed almost in all depth sections of the relocated events (Figure 5.4.d). The dominant range of depths dramatically decreases going towards the west of the cluster, from 3-16 km to 3-8 km. Besides, the slope of the seismic activity persists (~56°) towards the west. The fault plane solutions for Yalova Cluster have been resolved by Örgülü and Aktar (2001), Karabulut et al. (2002), Özalaybey et al. (2002). All the solutions provide north-dipping mechanisms changing between 34° and 72°, however, the majority of the mechanisms is confined within a range of 40° and 60°. The fault plane solutions also show that the strikes are mostly oriented in E-W direction. All of the fault plane solutions mentioned above reflect a good agreement with the characteristics of the activity in Yalova Cluster obtained by HypoDD.

Up to now, the seismicity of Yalova Cluster had never been associated with the presence of a single fault segment. However, the seismic activity obtained by HypoDD clearly represents the fault geometry as well as the seismogenic zone. This clear geometry is strongly supported by the fault plane solutions (Örgülü and Aktar, 2001; Karabulut et al., 2002; Özalaybey, 2002). Therefore, we claim that all of this information implies an existence of a normal fault dipping to the north (~56°) beneath the northern part of the Armutlu Peninsula. The existence of normal faults in the Marmara Sea was known for longtime. This is not surprising because Marmara Sea is partly deforming under the influence of the Aegean extension tectonics (J. R. Parke, 2002). The exact location and the rate of extension of normal faults within the Marmara Sea is less known since there was no significantly large earthquakes recorded on these normal faults. One single exception is the Çınarcık fault of 1963 where there are still many points that are left unclarified (location, depth, etc). Marine seismic surveys provided shallow structure data for the presence of E-W aligned normal faults along southern Marmara (Parke et al., 2002), however the present activity of these faults is still not known. The normal fault that we identify in Yalova using aftershocks is probably another exemple of normal fault that releases the extensional strain in the N-S direction. However, we feel that more evidences are needed in order to verify the claims explained above.

The Central Cluster is distributed roughly within a rectangular area of 65x7 km, 10 km east of the Hersek Peninsula and 15 km south of the Princes Islands. The activity is gradually terminated near 29.0°E. The event distribution of the Central Cluster exhibits linearity along the activity zone. Strictly speaking the epicenters are not confined with a very narrow zone. There are several reasons for observing the relatively scattered view of the Central Cluster around this linearity. First, the distances between the cluster and the receivers are much greater as compared to the other clusters. Additionally, the azimuthal control is also much weaker especially in the western and the eastern ends of the Central Cluster. It may also be unrealistic to expect that all aftershocks be located in a very narrow zone that corresponds to the main rupture line. The aftershocks triggered by the strong earthquakes can be scattered about the main fault because of the shattered structure surrounding the main trace of the fault. Moreover, this experiment has been conducted using the recordings in the period of 15 days. In our view, Central Cluster requires data set that covers longer periods in order to provide the seismic structure of this region in more detail. Finally, the 1-D approximation of the velocity model, in addition to all the factors listed above is the basic limitations of the location studies.

In the Central Cluster, the fault plane solutions mostly indicate the right lateral strike slip mechanisms (Örgülü and Aktar, 2001; Karabulut et al., 2002; Özalaybey, 2002). They strongly support the distribution of the activity orientated in E-W direction. They also show a good agreement with the main shock of 1999 Izmit Earthquake in terms of locations and fault plane solutions.

The continuation of the rupture beyond the west of the Hersek Peninsula was longtime a very controversial issue. In the light of seismicity and SAR interferometry based studies, there is a common belief that the western extension of the İzmit rupture continues to further west than the Hersek Peninsula (Karabulut et al., 2002; Özalaybey et al., 2002). Çakır et al. (2003) have carried out a study with the purpose of investigating the co-seismic and early post-seismic slip rate associated with 1999 İzmit Earthquake based on SAR interferometry data. They show that the İzmit rupture extends to 30 km west of the Hersek Peninsula into the Marmara Sea with continuously decreasing slip from 2 m to 0 m (Çakır et al. 2003). As can be seen in the Figure 5.7 d, the depth values dramatically become shallower than 8 km in the most western depth section of Central Cluster. This result implies the rupture itself might not extend over the total length of the aftershock activity (29.0E), might stop earlier (29.1). Taking everything into account, the activity of Central Cluster plays a significant role in identifying the continuation of NAF into the Marmara Sea.

Central Cluster obviously differs from the other clusters with its seismotectonical characteristics. The continuation of NAF throughout the Marmara Region is a very significant unknown for which many studies have been conducted for several decades. The activity of Central Cluster provides an explanation of a part of unknowns about the seismotectonical of the region. The linearity of Central Cluster is consistent with the main characteristics of rupture of 1999 İzmit Earthquake, thus it implies a long and rectilinear continuation of NAF in the Marmara Sea from the eastern end of İzmit Bay up to 29.1° E . This linear as well as relatively long seismicity also implies that there is no major discontinuity (step-over, branching, etc) along the activity of Central Cluster.

REFERENCES

Aktar, M., Özalaybey, S., Ergin, M., Karabulut, H., Bouin, M.-P., Tapırdamaz, C., Biçmen, F., Yörük, A., Bouchon, M., Spatial variation of aftershock activity across the rupture zone of the 17 August 1999 Izmit earthquake, Turkey, Tectonophysics 391, 325–334, 2004.

Armijo, R., Meyer, B., Navarro, S., King, G. C. P. and Barka, A., Asymmetric slip partitioning in the Sea of Marmara pull-apart: A clue to propagation processes of the North Anatolian Fault, Terra Nova, 14, 80-86, 2002.

Barka, A.A., The North Anatolian Fault Zone. Ann. Tecton. 6, 164–195, 1992

Bendat J. S., Piersol A. G., Random Data: Analysis and Measurement Procedures. WILEY-INTERSCIENCE, 1971.

Deichmann, N., and M. Garcia-Fernandez, Rupture geometry from high-precision relative hypocenter locations of microearthquake clusters, Geophys. J. Int. 110, 501–517, 1992.

Dodge, D., G. C. Beroza, and W. L. Ellsworth, Evolution of the 1992 Landers, California, foreshock sequence and its implications for earthquake nucleation, J. Geophys. Res. 100, 9865–9880, 1995.

Ito, A., High resolution relative hypocenters of similar earthquakes by cross-spectral analysis method, J. Phys. Earth 33, 279–294, 1985.

Ito, A., Ucer, B., Barış, S., Nakamura, A., Honkura, Y., Kono, T., Hori, S., Hasegawa, A., Pektas, R., and Işıkara, A. M., Aftershock Activity of the 1999 Izmit, Turkey, Earthquake Revealed from Microearthquake Observations. Bull. Seism. Soc. Am. 92, 1,418–427, 2002.

J. R. Parke, R. S. White, D. McKenzie, T. A. Minshull, J. M. Bull, I. Kuşçu, N. Görür, and C. Şengör, Interaction between faulting and sedimentation in the Sea of Marmara, western Turkey, Journal Of Geophysical Research, 107, 2002.

Karabulut, H., Bouin, M., Bouchon, M., Dietrich, M., Cornou, C., and Aktar, M., The Seismicity in the Eastern Marmara Sea after the 17 August 1999 Izmit Earthquake. Bull. Seism. Soc. Am. 92, 1,387–393 , 2002.

Kissling, E., W. L. Ellsworth, D. Eberhart-Philipps, and U. Kradolfer, Initial reference models in local earthquake tomography, J. Geophys. Res. 99, 19,635–19,646, 1994.

Lay, T. and Wallace, T., Modern Global Seismology, Academic Press, 1995.

Le Pichon, X., Sengör, A. M. C., Demirbag, E., Rangin, C., Imren, C., Armijo, R., Gorur, N., Cagatay, N., de Lepinay, B.M., Meyer, B., Saatcilar, R. ve Tok, B., The active main Marmara fault, Earth Planet Science Letters, **192**, 595-616, 2001.

Lees, J. M., Multiplet analysis at Coso geothermal, Bull. Seism. Soc. Am., 88, 1127–1143, 1988.

Lienert, B. R., and J. Havskov, HYPOCENTER 3.2 -A computer program for locating earthquakes locally, regionally and globally, Seis. Res. Lett., 66, 26-36, 1995

Lomax, A. & Snieder, R., Identifying sets of acceptable solutions to non-linear, geophysical inverse problems which have complicated misfit functions, Nonlinear Processes in Geophysics, 2, 222–227, 1995.

Menke, W., Geophysical data analysis: Discrete Inverse Theory, San Diego, Academic Press, 1989.

Okay, A.A., Kaşlılar-Ozcan, I., Imren, C., Boztepe-Güney, A., Demirbag, E., Kuycu, I., Active faults and evolving strike-slip basins in the Marmara Sea, northwest Turkey: a multichannel seismic reflection study. Tectonophysics 321, 189– 218, 2000.

Örgülü, G. ve Aktar, M., Regional moment tensor inversion for strong aftershocks of the August 17, Izmit earthquake (Mw=7.4), Geophysical Research Letters, **28**, 371-374, 2001

Özalaybey, S., Ergin, M., Aktar, M., Tapırdamaz, C., Biçmen, F. ve Yörük, A., The 1999 Izmit earthquake sequence in Turkey: seismological and tectonic aspects, Bulletin of Seismic Society of America, **92**, 376-386, 2002.

Poupinet, G., W. L. Ellsworth, and J. Frechet , Monitoring velocity variations in the crust using earthquake doublets: An application to the Calaveras Fault, California, J. Geophys. Res., 89, 5719– 5731, 1984.

Parsons, T., Shinji, T., Stein, R. S., Barka, A. and Dieterich, J. A., Heightened odds of large earthquakes near Istanbul: an interaction-based probability calculation, Science, 228, 661-665, 2000.

Prejean, S.,W. Ellsworth, M. Zoback, and F.Waldhauser, Fault structure and kinematics of the Long Valley Caldera Region, California, revealed by high-accuracy earthquake hypocenters and focal mechanism stress inversions, J. Geophys. Res., 107(B12), 2355, 2002.

Pujol, J., Comments on the joint determination of hypocenters and station corrections, Bull. Seism. Soc. Am. 78, 1179–1189, 1988.

Robert Reilinger, Nafi Toksoz, Simon McClusky, Aykut Barka, 1999 Izmit, Turkey Earthquake Was No Surprise, The Geological Society of America, 10, 1, 2000.

Rubin, A. M., D. Gillard, and J.-L. Got, Streaks of micro-earthquakes along creeping faults, Nature, 400, 635– 641, 1999.

Schaff, D. P., G. H. R. Bokelmann, G. C. Beroza, F. Waldhauser, and W. L. Ellsworth, High-resolution image of Calaveras Fault, California, seismicity, J. Geophys. Res., 107(B9), 2186, 2002.

Şengör, A.M.C., The North Anatolian transform fault: its age, offset and tectonic significance. J. Geol. Soc. London 136, 269–282, 1979.

Thomas Eisenlohr, The Marmara Poly-Project, 1997

Thurber, C.H., Earthquake locations and three-dimensional crustal structure in the Coyote Lake area, central California, J. Geophys. Res., 88, 8226, 1983.

Van Decar, J. C., and R. S. Crosson, Determination of teleseismic relative phase arrival times using multi-channel cross-correlation and least-squares, Bull. Seism. Soc. Am. 80, 150–169, 1990.

Waldhauser, F., and W. L. Ellsworth. A double-difference earthquake location algorithm: method and application to the northern Hayward fault, Bull. Seism. Soc. Am. **90,** 1353–1368, 2000.

Waldhauser, F., and W. L. Ellsworth, Fault structure and mechanics of the Hayward fault, California, from double-difference earthquake locations, J. Geophys. Res., 107(B3), 2054, 2002.

Wong, H.K., Ludmann, T., Ulug, T.A., Gorur, N., The Sea of Marmara: a plate boundary sea in an escape tectonic regime, Tectonophysics 244, 231–250, 1995.

Ziyadin Çakir, Jean-Bernard de Chabalier, Rolando Armijo, Bertrand Meyer, Aykut Barka, and Gilles Peltzer, Coseismic and early post-seismic slip associated with the 1999 Izmit Earthquake (Turkey), from SAR interferometry and tectonic field observations. Geophys. J. Int. 155, 93-110, 2003.